INFLUENCE OF URBAN SQUARES ON NEAR-FIELD DISPERSION OF AIR POLLUTANTS

by

Peter MANNINGER
/N9UGPH/

Submitted to the
Department of Fluid Mechanics of the
Budapest University of Technology and Economics
in partial fulfilment of the requirements for the degree of
Master of Science in Mechanical Engineering Modelling

May, 2011

Project Report in Major Project /BMEGEÁTMWD1/

Supervisor:
Márton BALCZÓ, assistant research fellow

Evaluation Team Members, advisors:
Márton BALCZÓ, assistant research fellow
Miklós BALOGH, research engineer
Dr. Tamás LAJOS, professor
Anikó RÁKAI, Ph.D. student
Dr. Jenő M. SUDA, assistant professor

Department of Fluid Mechanics
Faculty of Mechanical Engineering
Budapest University of Technology and Economics

DECLARATION

Full Name (as in ID):	Manninger Péter
Neptun Code:	N9UGPH
University:	Budapest Unversity of Technology and Economics
Faculty:	Faculty of Mechanical Engineering
Department:	Department of Fluid Mechanics
Major/Minor:	MSc in Mechanical Engineering Modelling Spec. in Fluid Mechanics (major) and Solid Mechanics (minor)
Project Report Title:	Influence of urban squares on near-field dispersion of air pollutants
Academic year of submission:	2010 / 2011 - II.

I, the undersigned, hereby declare that the Project Report submitted for assessment and defence, exclusively contains the results of my own work assisted by my supervisor. Further to it, it is also stated that all other results taken from the technical literature or other sources are clearly identified and referred to according to copyright (footnotes/references are chapter and verse, and placed appropriately).
I accept that the scientific results presented in my Project Report can be utilised by the Department of the supervisor for further research or teaching purposes.

Budapest, 13 May, 2011

_____
(Signature)

FOR YOUR INFORMATION

The submitted Project Report in electronic format can be found in the Library of the Department of Fluid Mechanics at the Budapest Univeristy of Technology and Economics. Address: H-1111 Budapest, Bertalan L. 4-6. „Ae" building of the BME.

ASSIGNMENT

MSc MAJOR PROJECT (BMEGEÁTMWD1)

Title:	**Influence of urban squares on near-field dispersion of air pollutants**
Author's name (code):	**Péter Manninger (N9UGPH)**
Curriculum :	MSc in Mechanical Engineering Modelling / Fluid Mechanics
Supervisor's name, title:	**Márton Balczó, assistant research fellow**
Affiliation:	Department of Fluid Mechanics / BME
Assistant supervisor's name, title:	-
Affiliation:	
Description / tasks of the project:	1/ Literature review of the influence of urban squares on flow and dispersion. 2/ Design of a simplified test case for the investigation of the effect of an urban square on dispersion 3/ LDV measurement of the test case in the NPL wind tunnel 4/ Discussion of measurement results The project can be continued as a Final Project focusing on detailed wind tunnel tests of a specific urban site in autumn 2011.
Handed out / Deadline:	**7th of February 2011. / 13th of May 2011.**

Budapest, 7th of February 2011.

…….
Head of Department

Received by:

The undersigned declares that all prerequisite subjects of the Major Project have been fully accomplished. Otherwise, the present assignment for the Final Project is to be considered invalid. Signed in Budapest, on the 7th of February 2011.

…….
Student

Budapest University of Technology and Economics
Faculty of Mechanical Engineering
Department of Fluid Mechanics

Hungary, 1111 Budapest, Bertalan L. u. 4-6.
Telefon: (36-1) 463-4072 Fax: (36-1) 463-3464
http://www.ara.bme.hu

ABSTRACT

The present thesis deals with the influence of urban squares on near field dispersion of air pollutants. This is an important field of fluid mechanics as flow characteristics and related contamination concentration distributions have to be known to fulfil the strictly controlled governmental limitation values.

First, a broad literature overview was prepared by collecting the related articles and reviewing them in a comprehensive table.

Then, a model square arrangement was contrived and investigated in a wind tunnel. Laser Doppler Anemometry was used for the velocity measurement, whose working principle and features were introduced. Before measuring the model arrangement, the proper inlet flow conditions had to be set to be able to carry out reliable measurements which agree with the wind conditions of urban areas.

After ensuring the proper inlet conditions, velocity measurements were implemented with the realised wooden model. Fulfilling the similarity criterions of the modelled and the real-life case, characteristics of a real urban flow field could be investigated by means of this model.

Further studies using numerical methods and further more detailed measurements with different wind directions are planned to be done in the next semester within the framework of the Final project. Measurements and numerical calculations will be compared, and they are expected to validate each other.

KIVONAT

A dolgozatban városi terek légszennyeződések terjedésére gyakorolt hatását vizsgáltuk. Ez egy fontos kutatási terület, mivel városi környezetben a különböző szennyezőanyagok koncentrációjára szigorú előírások vannak, és a szennyezőanyagok terjedése pedig szorosan függ a vizsgált területen kialakult áramlástól.

Először egy szakirodalmi kutatást végeztem, melynek során összegyűjtöttem a kapcsolódó tudományos cikkeket, és elkészítettem egy áttekintő táblázatot, összefoglalva a cikkek tartalmát és fontos eredményeit.

Ezután megterveztük egy városi tér modelljét, melyet a későbbiek során szélcsatornában mértünk. A sebességméréshez egy 2 komponensű lézeres alapú sebességmérő műszert (LDA) használtunk, melynek működését és jellemzőit a dolgozatban bemutattam. Mielőtt a modellen való méréseket megkezdhettük volna, be kellett állítanunk a városi környezetre jellemző sebesség-viszonyokat a szélcsatornában. Ehhez egy német szabvány útmutatásait vettük alapul.

Ezután lettek elvégezve a modellen a mérések, melynek nagy része azonban az idő rövidsége miatt a következő félévre maradt. A következő félévben a mérések mellett helyet kap a tér numerikus modellezése is, mely a mérési eredmények segítségével validálható, és lehetőséget kínál az áramlási és terjedési mechanizmusok teljesebb megértésére.

CONTENTS

DECLARATION ii
ASSIGNMENT iii
ABSTRACT iv
CONTENTS vi
NOMENCLAUTURE vii
LIST OF FIGURES viii
1. INTRODUCTION ..... - 1 -
2. LITERATURE REVIEW ..... - 2 -
3. MEASUREMENT LAYOUT ..... - 10 -
4. MEASUREMENT METHOD ..... - 12 -
4.1 General introduction of the LDA technique ..... - 12 -
4.2 Introduction of the TSI system ..... - 17 -
5. MEASUREMENT SETTINGS AND CONDITIONS ..... - 19 -
5.1 Possible settings of turbulence generator elements ..... - 19 -
5.2 Horizontal profile measurements ..... - 20 -
5.3 Vertical profile measurements ..... - 22 -
5.3.1 Velocity profiles ..... - 22 -
5.3.2 Turbulence profiles ..... - 23 -
5.3.3 Standard deviation profile ..... - 24 -
5.4 Results of measurement settings ..... - 25 -
6. MEASUREMENT RESULTS ..... - 28 -
7. SUMMARY ..... - 30 -
8. FUTURE PLANS ..... - 30 -
9. REFERENCES ..... - 31 -
10. APPENDIX ..... - 35 -

NOMENCLAUTURE

x direction along the wind tunnel, increasing in flow direction [*mm*]

y direction perpendicular to *x* in the horizontal plane [*mm*]

z vertical direction, increasing upward [*mm*]

$\underline{u}$ velocity vector [*m/s*]

u velocity component along the main wind directon (*x*) [*m/s*]

v lateral velocity component in (*y*) direction [*m/s*]

w vertical velocity component in (*z*) direction [*m/s*]

$\overline{u}$ time averaged velocity along the main wind directon (*x*) [*m/s*]

I turbulence intensity [*%*]

I_u turbulence intensity in *x* direction [*%*]

I_v turbulence intensity in *y* direction [*%*]

I_w turbulence intensity in *z* direction [*%*]

σ_u standard deviation of velocity component u [*m/s*]

σ_v standard deviation of velocity component v [*m/s*]

σ_w standard deviation of velocity component w [*m/s*]

z_{ref} reference height [*mm*]

u_{ref} velocity component u along wind direction at reference height [*mm*]

h height [mm]

z_0 roughness length [*mm*]

d_0 zero plane displacement [*mm*]

α profile exponent [-]

λ wave length of the laser light [*m*]

f frequency of the laser light [*1/s*]

f_D Doppler frequency [*1/s*]

LIST OF FIGURES

Figure 3.1: A real urban area – József Nádor tér ..... - 10 -
Source: http://maps.google.com
Figure 3.2: The 2D plan of the model ..... - 11 -
Figure 3.3: The CAD model and the realised wooden model ..... - 11 -
Figure 4.1: The intersection of laser beams ..... - 12 -
Source: [39]
Figure 4.2: The elements of the LDA ..... - 14 -
Source: [40]
Figure 4.3: Types of scattering ..... - 15 -
Source: [39]
Figure 4.4: The detected and the filtered signals ..... - 16 -
Source: [40]
Figure 4.5: The operation of the Bragg cell ..... - 16 -
Figure 4.6: The TSI LDA system ..... - 17 -
Source: [42]
Figure 4.7: The signal path of the LDA for one channel ..... - 17 -
Source: [41]
Figure 4.8: The FlowSizer software ..... - 18 -
Figure 5.1: The NPL wind tunnel of the department ..... - 19 -
Source: http://www.ara.bme.hu/cms
Figure 5.2: The adjustment of obstacles and spikes, and the measuring arrangement ..... - 19 -
Figure 5.3: Obstacles with different packing densities ..... - 20 -
Figure 5.4: Horizontal velocity profiles in case of default (upper left), isolated (upper right), and isolated and blocked (lower) arrangements ..... - 21 -
Figure 5.5: The undimensionalized and shifted result of the horizontal velocity profile measurements ..... - 21 -
Figure 5.6: Measured and calculated results of the vertical velocity profiles ..... - 23 -
Figure 5.7: The measured turbulence intensities ..... - 24 -
Figure 5.8: The measured RMS values along a vertical profile ..... - 25 -
Figure 5.9: The vector plot of the measured profiles ..... - 26 -
Figure 5.10: The vertical vector plot and interpolated w field ..... - 26 -
Figure 5.11: The interpolated velocity (left) and turbulence field (right) ..... - 27 -
Figure 6.1: The location of the examined vertical profiles ..... - 28 -
Figure 6.2: The side view of the velocity vectors with measurement points coloured by main velocity component (left) and main turbulence component (right) along the vertical profiles ..... - 29 -

1. INTRODUCTION

The topic of the thesis is the influence of urban squares on near-field dispersion of air pollutants. In densely inhabited urban areas, like in cities, squares are always present and they strongly affect the flow characteristics. They have an effect on the velocity field and on turbulence characteristics, which determine the dispersion of air pollutants, and the distribution of their concentration. These features are important to deal with, because there are strict limitations for the concentrations of certain materials in urban areas. Most important pollutants of traffic origin are NOx, NO2, PM10.

Initiated by a recent study of the department, which dealt with the velocity field and concentration distribution of a certain urban square in Budapest, we decided to examine a simplified arrangement of block houses around a square. The topic was divided into two part, one which deals with the flow and dispersion, measuring the velocity field distribution by an LDA system, and one, which deals with the concentration distribution of contaminations. Both studies examine the same model arrangement to gain connected information about flow characteristics and concentration distributions. This thesis deals with the flow measurement part of the above mentioned topic.

2. LITERATURE REVIEW

After revising the related articles it can be said that 5 typical arrangements can be found in the literature. There are ones which deal with a single cubical obstacle, and mainly investigate its downstream flow features. A cubical obstacle can be handled as the simplest arrangement of a single building. In case of real-life modelling arrangements, it is not enough to model a single building in its own, because the effect of the surrounding buildings cannot be neglected. But it has a great importance to understand how the flow behaves in the wake of a single building.

Enlarging the modelled scales, the next two arrangements are the canyon array and the street intersections. Both of them deal with an urban-like arrangement of a few simplified rectangular building. In the case of canyon array two blocks are investigated. They are parallel to each other and both of them are significantly longer in one horizontal direction, then in the other. Generally the cross flow is examined in this array (wind direction is normal to the longer horizontal direction). The other array is the street intersection, which deals with the flow inside a perpendicular street intersection, surrounded by 4 cubical blocks. Both approach deals with a picked out part of real urban areas.

The next type is the matrix of cubes, which tries to model the whole urban area in a very simplified case. It consists of a set of cubical buildings in two different arrays. The first is the aligned array of the buildings, which means that they are situated in the wake of each other, with a constant street width in both directions. The second one is the staggered array, when every second row is placed behind the gap of the buildings in front of them. Of course it is a very simplified test case, but the first approach to model an urban-like domain.

The last type is the real urban model, which models the buildings in context with each other at a reduced scale. The geometry is no more simple and standardised; it is the same as in reality. Generally they model from 5-10 up to 100-200 buildings in the same arrangement as that of the real buildings. This type gives the most precise approximation for real urban places.

In an article, Theurer (1999) [1] introduces the types of typical building arrangements. These types are: 1-2 stories single and double family buildings, 1-3 stories residential and commercial dense urban developments, 2-4 stories building rows and building blocks, block edge buildings with 2-4 stories, city centres, commercial areas, industrial areas, green areas

with few trees, and parks with trees and forest areas. Some parameters are introduced and specified to describe the geometry and arrangement of the above mentioned building types. These parameters are the average building height, height/street width ratio, average street length, spacing ratio of the streets, roof type and vegetation within the street. All parameters were defined in case of a small town with 50000 inhabitants, a medium-sized city with 160000 inhabitants and a large city with 300000 inhabitants. Later on we will use these parameters to describe our model.

After contriving a certain arrangement to investigate, one has to decide the approach of investigation. Basically we can measure or calculate the flow features. Measurement types can be the field measurement (1:1 scale, on the spot), wind tunnel and water tunnel measurements (both of them investigate a smaller model of the object). Calculations can be analytical or numerical calculations. Analytical calculations use the well-known governing equations of the fluids and any equations describing physical quantities. In numerical calculations one solves the governing equations on a numerical grid of the model using different numerical approaches like Reynolds-average Navier Stokes equations (RANS), Large-Eddy Simulation (LES), or Direct Numerical Simulation (DNS), and different dimensions like 2D and 3D. Software used for this purpose are e.g. Fluent, CFX, Miskam, Mercure, Code Saturne, OpenFoam.

All the above mentioned methods are good to validate each other. Hence, almost each article uses at least two of these methods. Generally, they use a numerical simulation and validate it with measurement. Another possibility is to use a former result of a same arrangement. Mentioning a few example, we can find field and wind tunnel measurement [6], [12], field measurement with numerical simulation [8], wind tunnel measurement with numerical simulation [9], [23], water tunnel measurement with numerical simulation [7], different numerical simulations [5], and even measurement and former results [27], [35], and numerical simulation and former result [2], [24].

In the following part of the literature review the important articles of this topic are going to be collected in a comprehensive table by defining their modelled field, their measurement type, giving a short description, and showing a figure of the investigated arrangement in the Appendix.

Title	Author	Type of meas.ment	Modeled field	Description	Picture
A comparison of Large Eddy Simulations with a standard k–e Reynolds-averaged Navier–Stokes model for the prediction of a fully developed turbulent flow over a matrix of cubes	Cheng et al.	LES &RANS	Matrix of cubes	Comparison of velocity profiles and velocity fields, time energy spectra for the velocity components	figure 1
A comparison of results from scaled field and wind tunnel modelling of dispersion in arrays of obstacles	Macdonald et al.	Wind tunnel & scaled field meas.ment	Matrix of cubes	Gaussian concentration distribution Variation of lateral diffusion parameter	figure 2
A methodology to urban air quality assessment during large time periods of winter using computational fluid dynamic models	Parra et al.	CFD	Pamplona, part of city	modeling large time periods, examining street intersections and a whole part of city	figure 3
A new urban boundary layer and dispersion parameterization for an emergency response modeling system: Tests with the Joint Urban 2003 data set	Monache et al.	Field meas.ment	Oklahoma City	meteorological data, urban boundary layer effect, rural and urban case, sensor measurements, concentration isosurfaces, pattern of correspondence between predictions and observations	figure 4
A numerical study of the effects of ambient wind direction on flow and dispersion in urban street canyons using the RNG k–e turbulence model	Baik et al.	RANS & wind tunnel	Matrix of cubes	Schematic of the mean flow circulation according to different wind directions, different flow patterns, flow and concentration fields	figure 5
A simple network approach to modelling dispersion among large groups of obstacles	Hamlyn et al.	Wind tun. & former studies	Matrix of cubes	Different building arrangements, diff. wind directions, tall building, Gaussian & lateral concentration profiles	figure 6
An improved method for the estimation of surface roughness of obstacle arrays	Macdonald et al.	-	-	Existing methods for estimating surface roughness, parameter	-

Title	Author	Type of meas.ment	Modeled field	Description	Picture
Comparisons of model simulations with observations of mean flow and turbulence within simple obstacle arrays	Macdonald et al.	LES & water tunnel	Matrix of cubes	Velocity profiles, examining different arrays and comparing each row of the arrays	figure 7
Computational Fluid Dynamics modelling of the pollution dispersion and comparison with measurements in a street canyon in Helsinki	Neofytou et al.	Field meas.ment & CFD	Helsinki, part of city	Concentration at street and roof level measured during a long period, concentration distributions and flow field	figure 8
Computer simulation of wind environmental conditions around buildings	Stathopoulos et al.	RANS & wind tunnel	Montreal, few buildings	Wind map, velocity field, turbulence profiles, relation between measured and computed velocity ratios	figure 9
Effects of inflow turbulence intensity on flow and pollutant dispersion in an urban street canyon	Baik et al.	2D numerical model	canyon	Examining inflow turbulence conditions on velocity field, flow changes with inflow turbulence intensity, velocity & turbulence profiles, concentrations	figure 10
Field and wind tunnel investigations of plume dispersion around single surface obstacles	Mavroidis et al.	Field & wind tunnel	Single cube	tracer gas – concentration measurement, flow visualization, plume is more dispersed in field	figure 11
Field experiments of dispersion through rectangular arrays of cubic structures	Macdonald et al.	Scaled field meas.ment	Matrix of cubes	Experimental parameters for concentration measurement, different wind directions and different arrays, Measurement in 9 field point	figure 12
Flow and dispersion in an urban cubical cavity	Baik et al.	RANS	Cubical cavity	velocity field inside the cube, particle trajectories, Turbulence parameters: TKE, Turbulence intensity	figure 13

Title	Author	Type of meas.ment	Modeled field	Description	Picture
Flow and dispersion in street intersections	Soulhac et al.	Wind tunnel & num. (FLUENT & Mercure)	Street intersection	Mean velocity profiles, flow streamlines and dispersion in street intersection at different wind directions, LDA meas.	figure 14
Flow over cube arrays of different packing densities	Cheng et al.	Wind tunnel	Matrix of cubes	Pressure coefficient and drag coefficient distributions, shear stresses profiles, different roughness, staggered/aligned array, different packing density, HWA	figure 15
Large-eddy simulation for flow and dispersion in urban streets	Castro et al.	LES, RANS & wind t.	London, part of city	RANS failed to predict the separation bubbles $\rightarrow$ LES, velocity profiles, pathlines concentration profiles	figure 16
Lateral channeling within rectangular arrays of cubical obstacles	Baik et al.	Water tunnel	Matrix of cubes	velocity field analysis, lateral channeling, tall building effect, PIV visualization,	figure 17
Local characteristics of atmospheric dispersion within building arrays	Mavroidis et al.	Wind tunnel	Matrix of different obstacles, tall building	Aligned/staggered array of different obstacles (cube 0 and 45 deg, cylinder, tall obstacle), different packing densities, tall building, diff. wind speed and direction, flow visualization, concentration profiles, PPM(time) functions	figure 18
Mean flow and turbulence statistics over groups of urban-like cubical obstacles	Castro et al.	DNS & wind tunnel	Matrix of cubes	Different arrangements, flow field, vorticity contours, pressure difference profiles, Reynolds stresses, Turbulent Kinetic Energy, drag coefficients, mixing lengths	figure 19

Title	Author	Type of meas.ment	Modeled field	Description	Picture
New inflow boundary conditions for modelling the neutral equilibrium atmospheric boundary layer in computational wind engineering	Chen et al.	Wind tunnel	Obstacles generating turbulence	Inflow velocity & turbulent BCs, Comparing fitted curves to measurement experimental data, calculating k & ε terms to RANS model	figure 20
Numerical and experimental modelling of the three-dimensional turbulent wind flow through an urban square	Gadilhe et al.	wind tunnel & RANS	Nantes, semi-circular square	Comp RANS & wind tunnel using HWA, velocity profiles, measurement difficulties in wakes behind buildings and recirculating zones	figure 21
Numerical simulation of flow and dispersion around an isolated cubical building - the effect of the atmospheric stratification	Mavroidis et al.	modified RANS, previous exp.ments	Isolated cube	Neutral, stable & unstable atmospheric conditions, modifications in k - ε model (inclusion of the Kato and Launder correction & modified wall function)	figure 22
On the use of the k–ε model in commercial CFD software to model the neutral atmospheric boundary layer	Hargreaves et al.	modified RANS, previous works	Wind tunnel domain	How to use k - ε model for the neutral ABL (only with modified law of the wall and with a shear stress applied to the top boundary of the domain). measures are suggested to moderate the decay of the BL	figure 23
Perspectives on air pollution aerodynamics	Meroney	-	-	general introduction to air pollution aerodynamics	-
Semi-empirical models as a combination of wind tunnel and numerical dispersion modelling	Theurer et al.	Semi-emp model compared to former results	Different building types	Different building arrangement types with different parameters, plume dispersion, semi empirical model to combine wind tunnel and numerical results	figure 24

Title	Author	Type of meas.ment	Modeled field	Description	Picture
Study of line source characteristics for 2-D physical modelling of pollutant dispersion in street canyons	Meroney et al.	Wind tunnel	Canyon	Setting inlet velocity profile, pressure taps, line source element, diff street canyon configurations, comp. between open country an urban case	figure 25
The effect of a tall tower on flow and dispersion through a model urban neighborhood, Part 1. Flow characteristics	Brixey et al.	Wind tunnel & LES	Tall building, Brooklyn	Longer blocks, flow visualization, LDV measurement, velocity fields in every plane, pressure coefficient distribution	figure 26
The effect of a tall tower on flow and dispersion through a model urban neighborhood, Part 2. Pollutant dispersion	Brixey et al.	Wind tunnel & LES	Tall building, Brooklyn	Time dependent concentration measurement methods, tall building effect, concentration isosurfaces	figure 27
The effect of surroundings with different separation distances on surface pressures on low-rise buildings	Meroney et al.	Wind tunnel & RANS	Matrix of cubes, one building	Roughness elements, inlet velocity and turbulence profiles, pressure coefficient distribution on the roof of a building	figure 28
Two-dimensional numerical modeling of flow and dispersion in the presence of hill and buildings	Baik et al.	RANS	Canyon and hill	The effect of a hill and/or 2 building (canyon) on the flow and pollutant dispersion, streamline fields	figure 29
Typical building arrangements for urban air pollution modelling	Theurer		Cities in Germany	Typical building arrangements, introduces parameters to describe them, vegetation in street canyon	figure 30
Wind-tunnel and numerical modeling of flow and dispersion about several building shapes	Meroney et al.	Wind tunnel & RANS	Several building shape	Different rectangular shapes & canyon, location of flow structures, pressure coefficient distribution on surfaces, concentration isopleths	figure 31

Title	Author	Type of meas.ment	Modeled field	Description	Picture
Wind tunnel measurements of concentration fluctuations in an urban street canyon	Pavageau et al.	Wind tun. & former studies	Canyon	70 sampling location, spatial distr. of mean concentration and concentration fluctuations, comparison with earlier results	figure 32
Wind tunnel simulation studies on dispersion at urban street canyons and intersections—a review	Ahmada et al.	Wind tunnel	Canyon, street intersect.	Flow regimes, flow characteristics at different aspect ratios, wake interference flow/skimming flow, concentration distr. with different traffic conditions, effect of vehicular motion on exhaust dispersion	figure 33
Wind tunnel simulations of plume dispersion through groups of obstacles	Davidson et al.	Wind tun. & former study	Matrix of cubes	Aligned/staggered configuration, velocity profiles, Gaussian and lateral concentration profiles	figure 34

3. MEASUREMENT LAYOUT

This section introduces the planning and designing steps of the model arrangement. The goal was to create a measurement layout similar to real urban squares to receive a general idea about flow patterns inside a square. The topic is really important in real life to see how a square ventilates according to ambient wind directions and wind speed and how the concentration of any contamination changes.

In the inner city of Budapest there are many densely inhabited areas with blocks of houses, and often the square itself is a missing block. This arrangement of block houses can be seen for example in József Nádor tér, in the fifth district of Budapest.

Figure 3.1: *A real urban area – József Nádor tér*

The aim of the model creation was to create a general and simplified model, which is at the same time similar to the upper introduced urban square. The most important parameters of such square are the length - width ratio of the blocks, the block height - street width ratio, and the block height - block thickness ratio. Defining these parameters of the introduced urban square we constructed the geometry of the model as follows.

We got two different types of building blocks: blocks with quadratic shape in the ends of the square, and two rectangular shape blocks with 1:3 side ratio along the square. The block height – block thickness ratio was 2:1 and the block height – street width ratio was also 2:1.

Similarly we had to decide the size of the model according to the measurement volume of the wind tunnel. Taking the street width to 15 meter from map, we received the other sizes of the square, and calculated the biggest model size, which is possible to be measured in the wind tunnel. Achieving the biggest possible size of the model is important to see more clearly

the flow patterns of the inside the square. This way the ratio of the modelled and the real urban square became 1:650. The sectional view of the model with the sizes can be seen in figure 3.3.

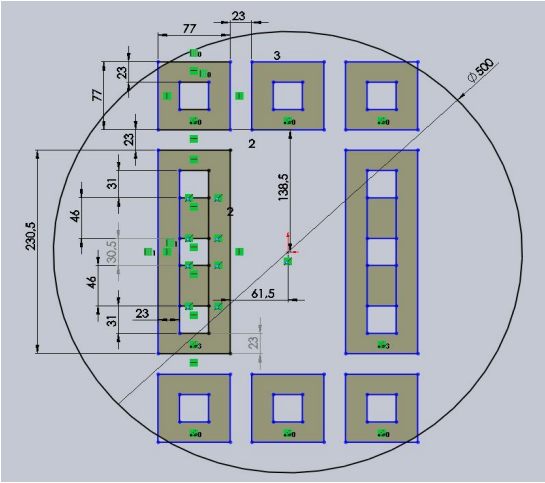

Figure 3.2: *The 2D plan of the model*

The model was prepared from wooden material, the blocks were stuck together from properly cut pine laths, and were stuck onto a milling cut 9mm thick laminated circular disc. Afterwards, the gaps and leaks were filled up with a silicone sealing-compound, and the whole model was polished. Finally it was painted to black to prevent the reflection of the laser light, which could fake the measurement results. The 3D plan of the model and the realized wooden model are shown in the figure 3.2.

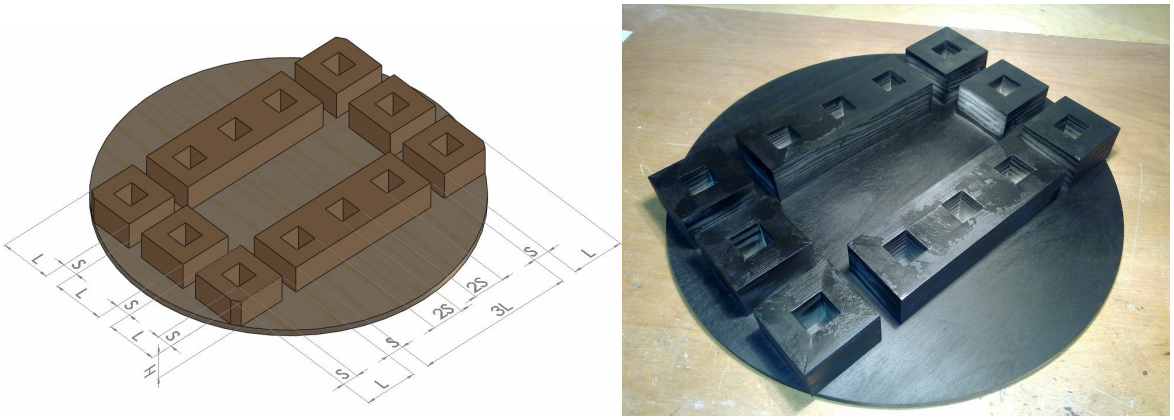

Figure 3.3: *The CAD model and the realised wooden model*

4. MEASUREMENT METHOD

4.1 General introduction of the LDA technique

For the wind tunnel measurements Laser Doppler technique, most frequently referred to as Laser Doppler Anemometer (LDA) or Laser Doppler Velocimeter (LDV) was used. This is a non-contact, particle based, point-wise velocity measurement technique, which requires optical access to the measurement volume, and tracer particles to follow reliably the flow and all velocity fluctuations. For calculating a certain component of the velocity the device uses two laser beams crossing each other in the measurement volume. When a particle is moving through this intersection, it scatters the light back, and the scattered light frequency is linearly proportional to its velocity.

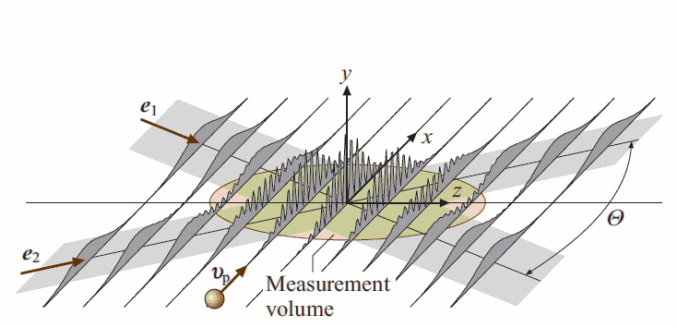

Figure 4.1: *The intersection of laser beams*

We have two approaches to explain the working principle and to calculate the velocity of the particle. These two models give the same result.

The first approach is called the fringe model. As the two laser beams are coherent, interference occurs in the intersection, with an interference fringe pattern. This fringe pattern provides the necessary light pattern to illuminate the particles. When a particle moves across these fringes, a periodic light-intensity signal will be generated, and the backscattered light frequency will be proportional to the velocity component perpendicular to these fringes. As the fringe spacing can be calculated exactly from the wavelength of the light and the half angle of the beams, the velocity can also be calculated directly from the measured frequency. The fringe spacing distance can be calculated as follows:

$$d_f = \frac{\lambda}{2 \cdot \sin\frac{\alpha}{2}}, \tag{4.1}$$

where d_f is the fringe spacing distance, λ is the wavelength of the laser light, and α is the angle between the two laser beam. From this we receive the corresponding velocity component, perpendicular to the fringes: $$u_\perp = d_f \cdot f = \frac{\lambda}{2 \cdot \sin\frac{\alpha}{2}} \cdot f\,, \tag{4.2}$$

where $u_\perp$ is the corresponding velocity component, and f is the detected frequency.

The second approach is the Doppler model. When we use only one laser beam, which illuminates a moving particle in the flow, then this particle movement creates a Doppler shift in the light frequency directly proportional to its velocity. If we use two laser beams, each will create a Doppler effect on the moving particle, and the scattered light from the particle will mix at the photodiode, which receives the reflections from both laser beams. At the interference of two light signals of nearly the same frequency, one gets a low frequency called beat frequency which is half of the difference of both frequencies. This frequency is low enough to be detected by an electric data acquisition system. Thus, from the measurement of this Doppler shift frequency one can determine the particle's velocity.

The Doppler shifted frequency of a single laser beam when the wave source and the observer hold their position, and the transmitter is moving can be calculated in the following way if $u << c$:

$$\begin{aligned}
&f' = f \cdot \frac{1 - \frac{1}{c} \cdot \underline{u} \cdot \underline{e}_1}{1 - \frac{1}{c} \cdot \underline{u} \cdot \underline{e}_2} = f \cdot \left(\frac{1}{1 - \frac{1}{c} \cdot \underline{u} \cdot \underline{e}_2} - \frac{\frac{1}{c} \cdot \underline{u} \cdot \underline{e}_1}{1 - \frac{1}{c} \cdot \underline{u} \cdot \underline{e}_2} \right) \cong \\
&f \cdot \left[\left(1 + \frac{1}{c} \cdot \underline{u} \cdot \underline{e}_2 \right) - \frac{1}{c} \cdot \underline{u} \cdot \underline{e}_1 \cdot \left(1 + \frac{1}{c} \cdot \underline{u} \cdot \underline{e}_2 \right) \right] = \\
&f \cdot \left(1 + \frac{1}{c} \cdot \underline{u} \cdot \underline{e}_2 - \frac{1}{c} \cdot \underline{u} \cdot \underline{e}_1 - \frac{1}{c} \cdot \underline{u} \cdot \underline{e}_1 \cdot \frac{1}{c} \cdot \underline{u} \cdot \underline{e}_2 \right) \cong \\
&f + f \cdot \frac{1}{c} \cdot \underline{u} \cdot (\underline{e}_2 - \underline{e}_1),
\end{aligned} \tag{4.3}$$

where f' is the Doppler shifted frequency, f is the initial frequency, c is the speed of light, $\underline{u}$ is the velocity vector, $\underline{e}_1$ is the vector between the wave source and the transmitter, and $\underline{e}_2$ is the vector between the transmitter and the observer. Then the frequency change will be:

$$\Delta f = f - f' = \frac{f}{c} \cdot \underline{u} \cdot (e_1 - e_2) = \frac{\underline{u}}{\lambda} \cdot (e_1 - e_2) \tag{4.4}$$

In case of two laser beams the reflected signals will interfere and a beat frequency will appear from the two Doppler frequencies:

$$f_D = \frac{\Delta f_1 - \Delta f_2}{2} = \frac{f_2' - f_1'}{2} = \frac{1}{2} \cdot \left(f \cdot \frac{1 - \frac{1}{c} \cdot \underline{u} \cdot \underline{e}_1}{1 - \frac{1}{c} \cdot \underline{u} \cdot \underline{e}_3} - f \cdot \frac{1 - \frac{1}{c} \cdot \underline{u} \cdot \underline{e}_2}{1 - \frac{1}{c} \cdot \underline{u} \cdot \underline{e}_3} \right) = \frac{\underline{u}}{2\lambda} \cdot (\underline{e}_2 - \underline{e}_1), \quad (4.5)$$

where $\underline{e}_1$ is the vector between the transmitter of beam 1 and the observer, and $\underline{e}_2$ now is the vector between the transmitter of beam 2 and the observer, and $\underline{e}_3$ is the vector between the transmitter and the observer. In practical measurement setups, 2 f_D can be measured as the reflected light intensity is a squared value of amplitude and thus 90° and 270° phases both give positive intensity peaks, resulting in double frequency. The huge advantage is that the Doppler shifted frequency f_D does not depend any more on the position of the photodetector, just from the position of the beam sources, which is a constant value according to the optical setup. For this, we can say, that:

$$\frac{\underline{e}_2 - \underline{e}_1}{2} = \sin \frac{\alpha}{2} \quad (4.6)$$

Thus we get the same result for the corresponding velocity component, which is the component perpendicular to the symmetry axis of the two laser beams, as before:

$$f_D = \frac{\underline{u}}{2\lambda} \cdot (\underline{e}_2 - \underline{e}_1) = \frac{1}{2\lambda} \cdot u_\perp \cdot 2 \cdot \sin \frac{\alpha}{2} \quad \Rightarrow \quad u_\perp = \frac{f_D \cdot \lambda}{\sin \frac{\alpha}{2}} = \frac{f_m \cdot \lambda}{2 \cdot \sin \frac{\alpha}{2}}, \quad (4.7)$$

where $u_\perp$ is the corresponding velocity component, perpendicular to the symmetry axis of the two laser beams and f_m is the measured frequency.

So the Doppler model gives the same result as the fringe model.

Now the components of the LDA are going to be introduced. These components are the laser beam generator, the beam separator, the fiberoptic probe, the photodetector, and the signal processor. Figure 4.2 shows these elements:

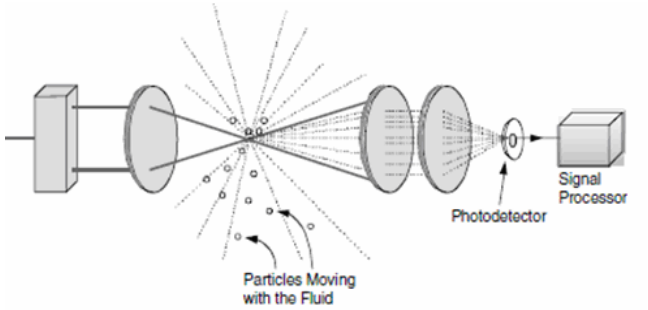

Figure 4.2: *The elements of the LDA*

The laser beam generator generates a coherent Gaussian laser beam, which goes into the beam separator. The beam separator generates the laser beam pairs of different frequency required for one-, two- or three-component LDA system by means of semi-permeable prisms, or by a rotating diffraction lattice. A shift in the frequency of one component of a laser beam pair also happens here (discussed later).

Then the laser beams are transmitted to the fiberoptic probe, which focuses all the laser beams into a certain point in the measurement volume. The measurement is realized at that certain point where all laser beams intersect each other. The moving seeder particles, whose movements have to be guaranteed to be the same as that of the flow, are passing through this measurement volume and scatter a Doppler-shifted light.

The Doppler-shifted light is going to be detected by the photodetector. According to the position of the photodetector we distinguish back scattering, forward scattering and side scattering LDA systems. The schematic of these systems are illustrated in figure 4.3.

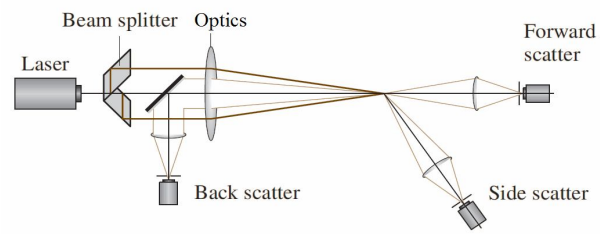

Figure 4.3: *Types of scattering*

The photodetector converts optical signals to electronic signals and also separates the different frequencies corresponding to a certain velocity component.

Finally, the signal processor postprocesses the incoming electric signal by means of different filters. All relevant information are calculated by examining the input signal at a certain sampling frequency, and transmitted to a PC for further postprocessing.

Moreover, it is important to say some words about the features of the detected scattered light, and its filtering. The light scattered from one certain moving particle is called “burst”. To detect a certain burst frequency, which is proportional to the velocity of the moving particle in the flow, the burst has to be identified from the continuous intensity signal, detected by the photodetector. This is done by setting proper trigger levels for the data recorder unit. In this way the data recorder only stores the “fly-by” of particles. After receiving the burst, Fourier transformation or auto correlation is carried out to determine the burst frequency. The intensity variation of a burst in time is shown in figure 4.4, where figure

“a” is the unfiltered, figure “b” is the high pass filtered and figure “c” is the low pass filtered signal. This signal is then transmitted for further analysis.

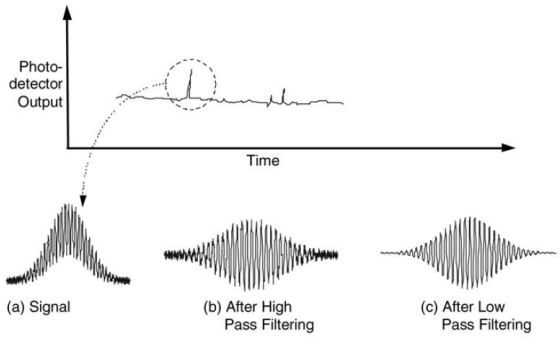

Figure 4.4: *The detected and the filtered signals*

After the analysis of a certain burst, we get a scalar value for one velocity component at a certain time instant. For a detailed pointwise measurement we need thousands of scalar velocities received from seeder particles. The measured velocities show a Gaussian distribution. The necessary number of measured scalar velocities depends on statistical rules and measurement requirements. The time of measuring at a certain point can vary from a few seconds up to several minutes.

To be able to distinguish between positive and negative velocities and to be able to measure around zero velocities (where the frequency should tend to zero) a shift is occurred in one component of the laser beam pair. By this shift, interference fringes move into the direction of the shifted beam, and the detected frequency at zero velocity will be the frequency shift. The shift of laser beam frequency is realized by means of a rotating diffraction lattice, or a so called Bragg cell (acousto-optic modulator). The Bragg cell is a mechanically (piezoelectrically) excited crystal, which behaves like an optical lattice according to the periodic density variation. The frequency shift of the laser beam is equal to the excitation frequency. The operation of the Bragg cell can be seen in figure 4.5.

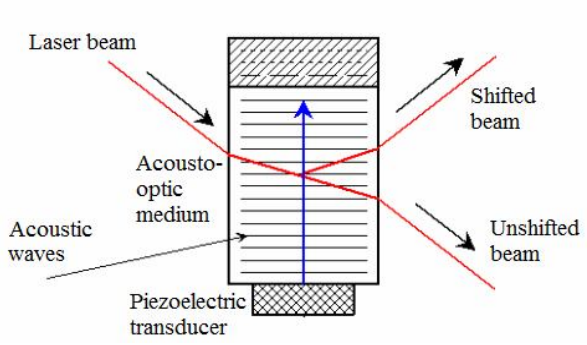

Figure 4.5: *The operation of the Bragg cell*

4.2 Introduction of the TSI system

TSI is one of the major manufacturers of LDA systems. The department has recently bought a 2-component TSI LDA system, which served as the velocity measurement device for our measurements. The device consists of the earlier introduced components, shown in figure 4.5.

Figure 4.6: *The TSI LDA system*

The TSI system has backscattering photo detection, detected with the same fiberoptic probe, which does the focusing of the beams. The device uses an adjustable Bragg cell for frequency shift. The detected optical sign is transmitted to the Photo Detector Module (PDM 1000), from where it is sent to the Signal Processor (FSA 4000). The steps of signal processing are sketched in figure 4.6.

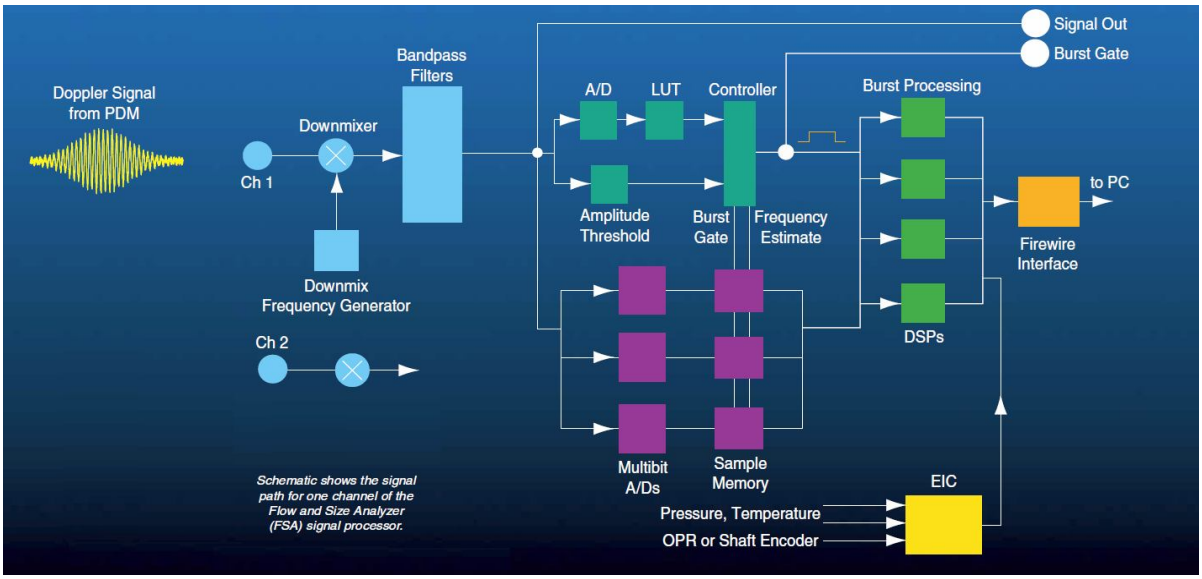

Figure 4.7: *The signal path of the LDA for one channel*

First, in the signal processor the incoming signal from the photodetector is downmixed with a signal of variable frequency to obtain a desired frequency backshift. The output of the downmixer is then sent through a bandpass filter and on the burst detector.

The burst detector uses a technique that combines Discrete Fourier Transform (DFT) and Look-up Tables (LUT) to attain on-line burst detection based on signal-to-noise ratio (SNR). An amplitude threshold is also used to enhance the burst detection capability. Another function of the burst detector is to estimate the frequency of the detected burst. This frequency estimate, combined with a burst gate signal which identifies the beginning and the end of the burst, is used to optimize burst sampling.

The incoming signals are also sampled, in parallel with burst detector, using multibit A/D converters. The frequency estimate provided by the burst detector determines which sampler is the best for the actual burst frequency. In addition, the burst gate identifies the best region of the burst from which to collect samples.

Then the best portion of the sampled bursts is processed to get the frequency by means of a Multiple Digital signal processor (DSP) chips using auto correlation. The informations are then sent to a PC and are going to be displayed by a software called FlowSizer. The setup, control, and operation are carried out by this software. It analyses the results and enable detailed display of them. Results can also be exported for further postprocess.

The screen of the software is shown in figure 4.7.

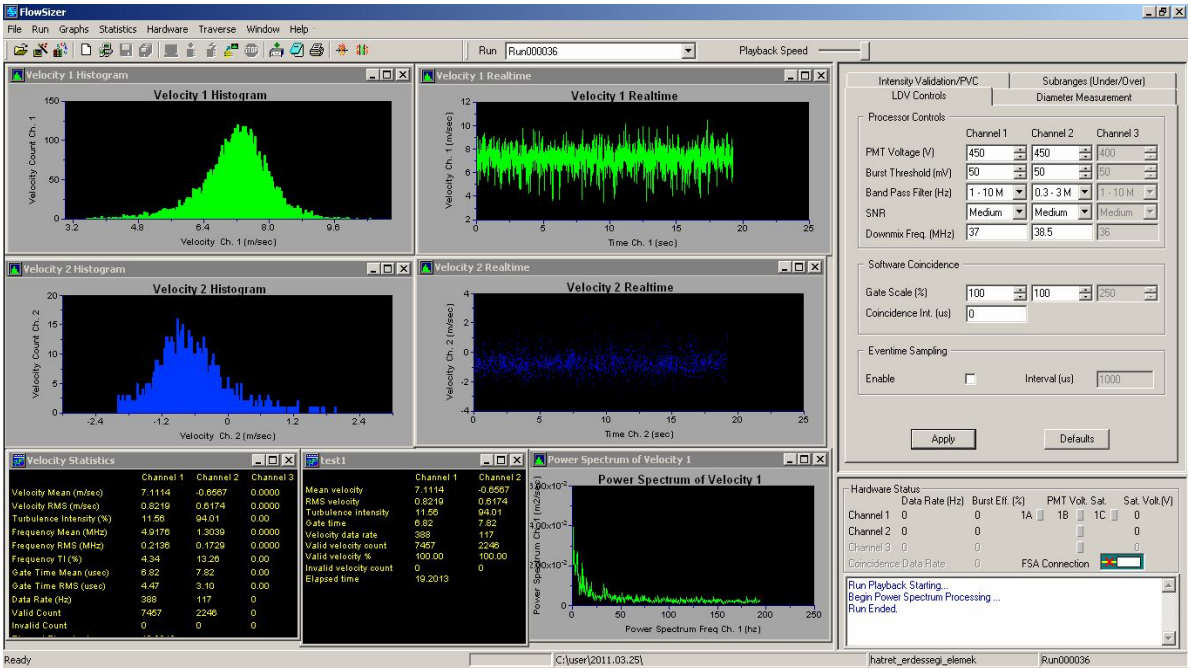

Figure 4.8: *The FlowSizer software*

5. MEASUREMENT SETTINGS AND CONDITIONS

5.1 Possible settings of turbulence generator elements

Every measurement took place in the NPL (National Physical Laboratory type) wind tunnel of the department. It is a wooden wind tunnel with 16 m/s maximal speed and a smallest turbulence intensity of 1%. It has a closed measurement section with a cross section of 0.5 x 0.5 m^2. The wind tunnel can be seen in figure 5.1.

Figure 5.1: *The NPL wind tunnel of the department*

To be able to perform reliable measurements of a modelled urban square, urban type inlet flow conditions has to be ensured in the wind tunnel. The atmospheric boundary layer's parameters are well known from scientific measurements (VDI 3783 guideline, [38]). The most important characteristics of urban like flow conditions to fulfil, are the proper inlet velocity and turbulence profiles. To generate the required conditions, rectangular obstacles were place into the flow onto the ground, and spikes were fixed behind them to generate a turbulent boundary layer flow. The arrangement of these elements and the measuring layout is shown in figure 5.2.

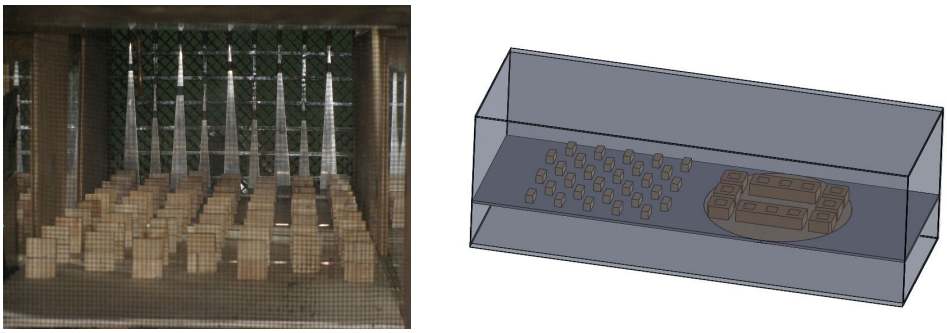

Figure 5.2: *The adjustment of obstacles and spikes, and the measuring arrangement*

To get the best possible set of the upper introduced rectangular obstacles, different arrangements with different packing densities and with different obstacle height have been tested. These tests are going to be introduced in the following subchapters. The different packing densities can be seen in figure5.3.

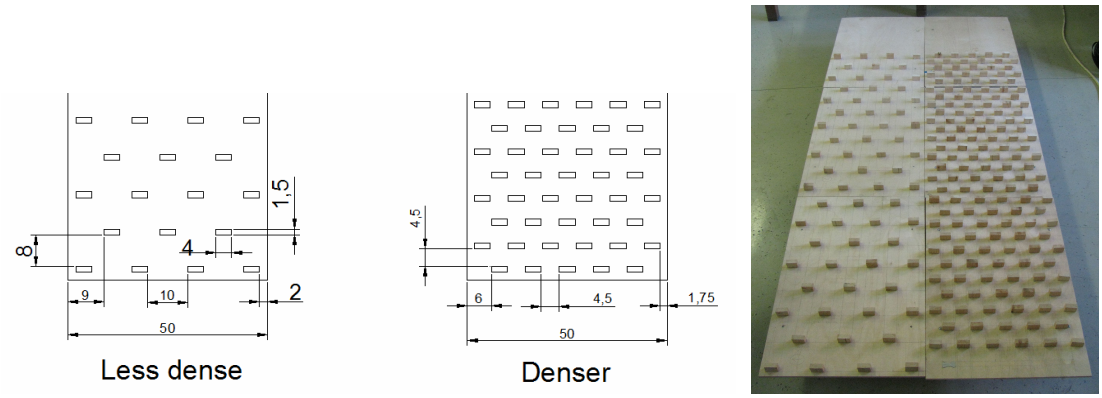

Figure 5.3: *Obstacles with different packing densities*

5.2 Horizontal profile measurements

First, horizontal profile measurements were carried out, at the original arrangement of the rectangular obstacles (denser arrangement, $h = 25\,mm$), still without the model. The goal was to adjust the wind tunnel settings. Three different measurements were carried out. One without any further setting of the wind tunnel, one with isolating the lacks between the platform and the wind tunnel walls, and one with isolation and also blocking the flow below the platform. By the isolation, leak flow could be eliminated, and by blocking the flow in the lower region, more homogeneous flow field was expected in the measurement section. The profiles were measured from the symmetry axis of the measurement section (y position is 0 *mm*) to the side wall of the wind tunnel (y position is 250 *mm*), supposing symmetrical flow characteristics.

The parameters to examine was that how uniform is the velocity in main flow direction (u) along the points of a vertical profile, and how this velocity profile brakes down close to the wall region. It was found, that the best arrangement is the isolated and blocked one, where the velocities along a profile was nearly constant and the breakdown close to the wall was less sharp. The measurement results are represented in figure 5.4.

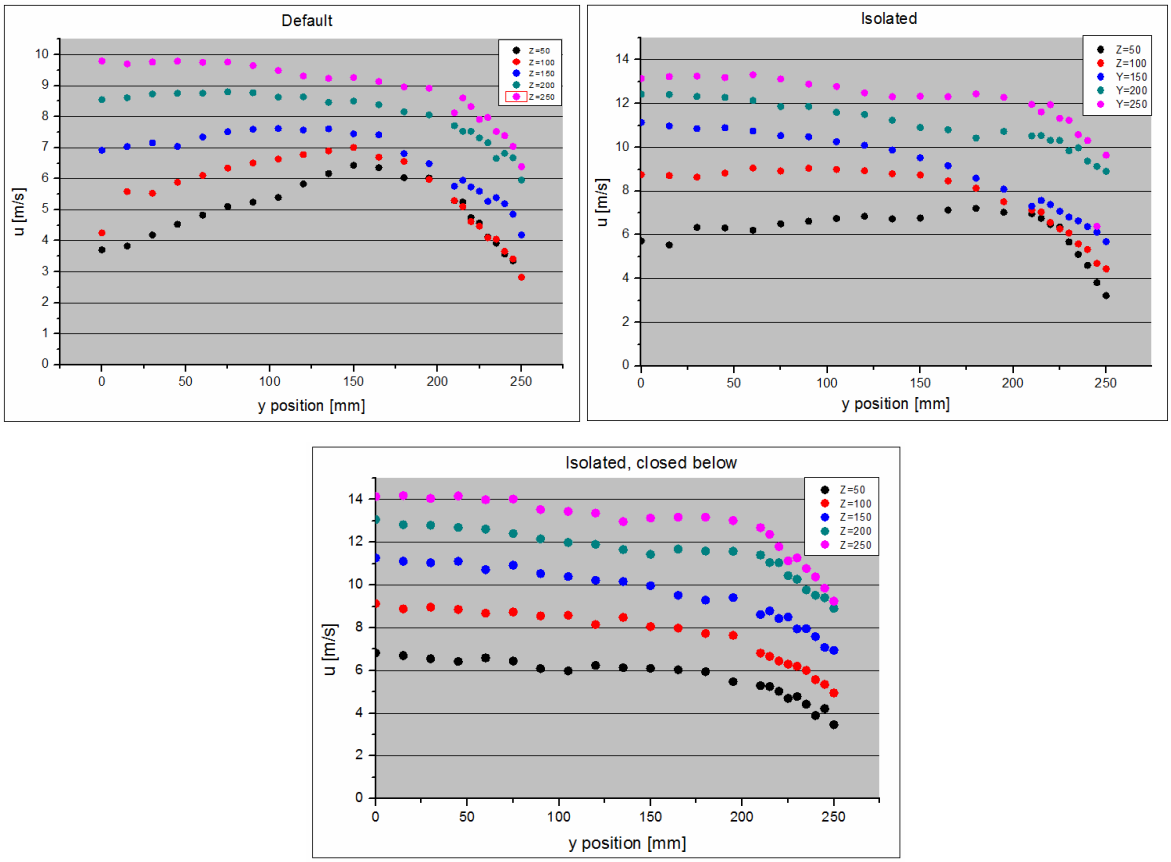

Figure 5.4: *Horizontal velocity profiles in case of default (upper left), isolated (upper right), and isolated and blocked (lower) arrangements*

These results can be illustrated within the same diagram undimensionaling the profiles with the first value, and shifting them according to their height in measurement section to have an easier comparison of them. Figure 5.5 demonstrates these profiles.

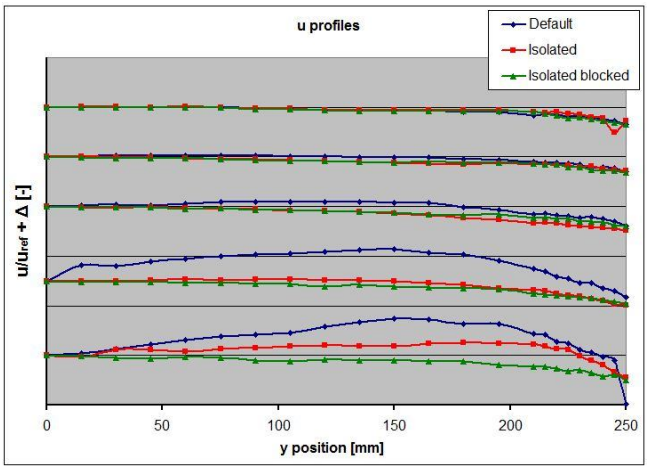

Figure 5.5: *The undimensionalized and shifted result of the horizontal velocity profile measurements*

We can see how the profiles get relaxed and become more uniform and similar to each other at higher positions, moving away from the boundary layer generator elements.

5.3 Vertical profile measurements

5.3.1 Velocity profiles

Next, vertical profile measurements were carried out to be able to compare our results with the required, calculated velocity profiles. There are different standards and guidelines to calculate the vertical velocity profile of the atmospheric boundary layer in case of different types of terrain, from the slightly rough water surface up to the very rough densely inhabited urban area. For this purpose, we used a German standard (VDI 3783 Part 12. [38]). According to this standard, the vertical profile of the time-averaged velocity $\bar{u}(z)$ can be approximated in two different ways:

$$\bar{u}(z) = u_{ref} \cdot \left(\frac{z - d_0}{z_{ref} - d_0} \right)^{\alpha}, \text{ or } \quad \bar{u}(z) = \frac{u_f}{\kappa} \cdot \ln\left(\frac{z - d_0}{z_0} \right), \tag{5.1}$$

where z is the height above the ground, z_{ref} is a reference height, z_0 is the roughness length, d_0 is the zero plane displacement, u_{ref} is the average wind velocity at reference height, u_f is the friction velocity, α is the profile exponent, and κ is the von Kármán's constant $\cong 0.4$. Close to the ground, the logarithmic formula is recommended.

According to the standard, one can choose the parameters required for different types of terrains. The values of the parameters are indicated in table 5.1.

Table 5.1: *Parameters of the equations (5.1) for different types of terrain*

Roughness class	**slightly rough**	**moderately rough**	**rough**	**very rough**
Type of terrain	ice, snow, water surface	grassland, farmland	park, suburban area	forest, inner city area
z_0 [m]	10^{-5} to $5 \cdot 10^{-3}$	$5 \cdot 10^{-3}$ to 10^{-1}	0.1 to 0.5	0.5 to 2
d_0 [m]	~ 0	~ 0	$\sim 0.75 \cdot h$	$\sim 0.75 \cdot h$
α [-]	0.08 to 0.12	0.12 to 0.18	0.18 to 0.24	0.24 to 0.4

In table 5.1 h is the building height in the suburban area or in the city. For our model, which is an inner city area, the very rough part is needed. So the chosen parameters are: $z_0 = 2\,m$, $d_0 = 0.75 \cdot 30 = 22.5\,m$, $\alpha = 0{,}32$.

The calculated results using these parameters of equation (5.1) are shown together with two measurement results in figure 5.6. The first measurement is in the case when the rectangular obstacle height was $h = 25\,mm$, and the second one is when it was doubled.

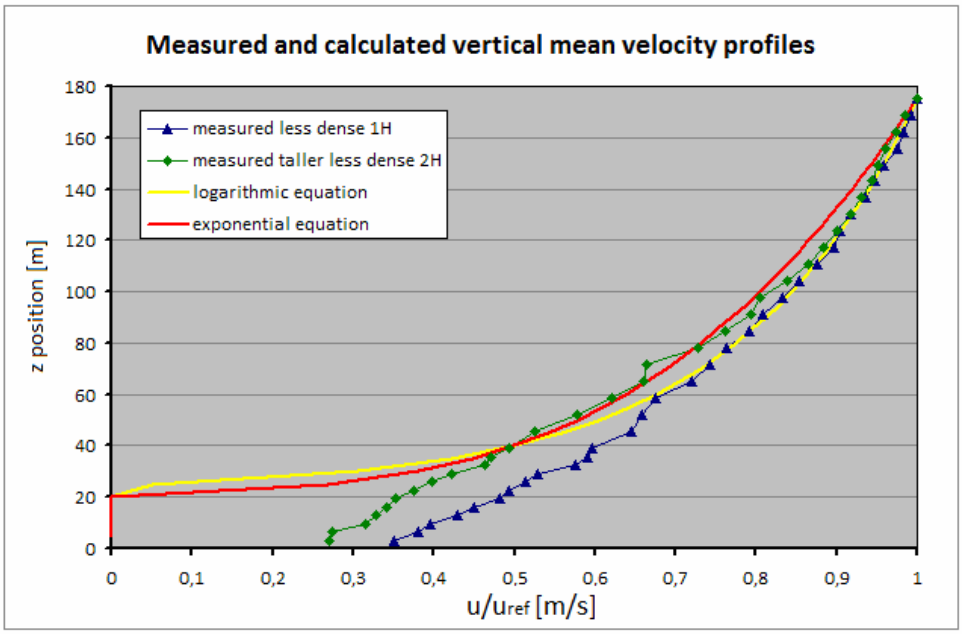

Figure 5.6: *Measured and calculated results of the vertical velocity profiles*

It can be seen, that above a certain height, both profiles converge to the theoretically calculated ones. At the height of the doubled rectangular boundary layer generator elements (50 mm height in model scale, 32.5 m height in real scale) the profiles are acceptably close to the required ones. (The calculated equations are only valid over the height of the buildings, which was $h = 30\,m$).

5.3.2 Turbulence profiles

Similarly to the velocity profiles, the standard has a specification for the horizontal turbulence profiles too. It specifies a range for each type of roughness class. Several measurements were carried out with different obstacle densities and obstacle height to check this turbulence criterion. We made measurements using the less dense arrangement with $1 \cdot h$ obstacle height ("Y=0, 1H" and "Y=50 1H"), with $2 \cdot h$ obstacle height ("Y=0, 2H" and "Y=50 2H"), with $2 \cdot h$ obstacle height and an additional horizontal vortex generator spike ("Y=0, 2H horiz" and "Y=50 2H horiz"), with $5 \cdot h$ obstacle height in the first two row and $2 \cdot h$ in the others ("Y=0, 5H" and "Y=50 5H"), and finally one with the denser configuration

at $y = 0\,mm$ ("original density). Profiles were measured in the symmetry plane of the wind tunnel ($y = 0\,mm$) and 50 mm closer to the side wall ($y = 50\,mm$). The results of the measurement of turbulence intensity in x direction are shown in figure 5.7.

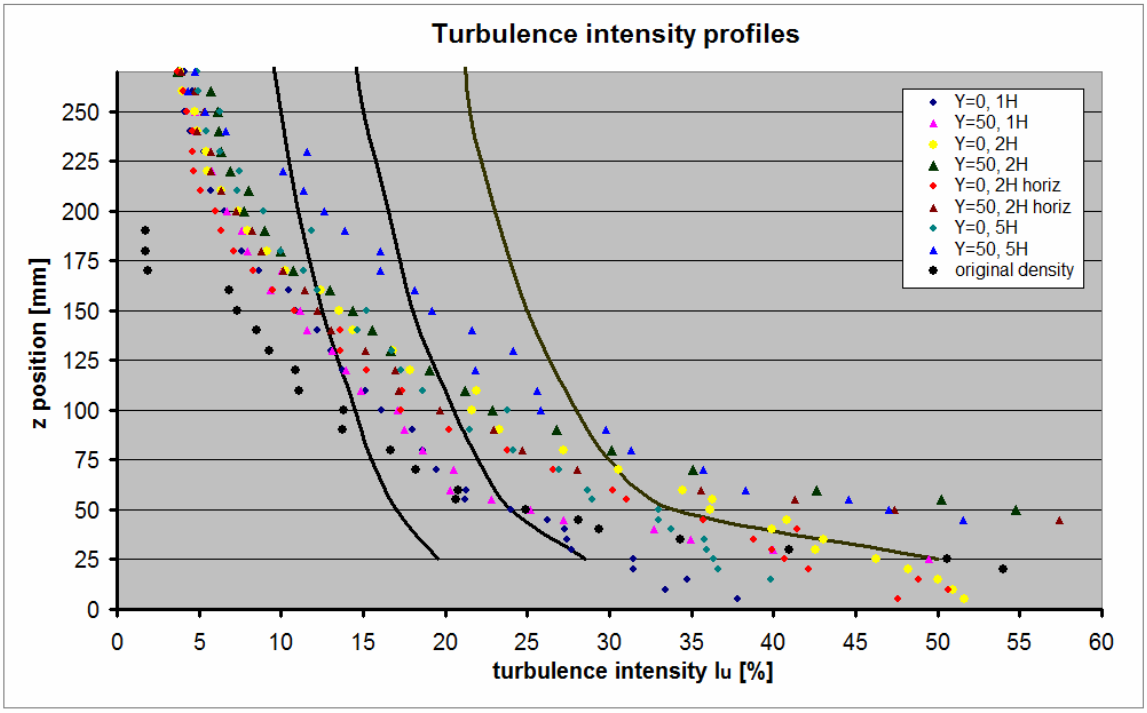

Figure 5.7: *The measured turbulence intensities*

We can see that the measurements do not show such a good agreement with this criterion as with the previous one. Unfortunately the agreement with the inner city and suburban area can only be guaranteed in the lower region, up to $\sim 150\,m = 5 \cdot h$.

According to the results of the vertical profile velocity and turbulence measurements the less dense arrangement with double height (50 mm) of rectangular boundary layer generator elements was chosen. This arrangement showed the best agreement with the required guidelines, which can be analogous to our expectation, as the height in this case was close to the height of the model ($h_{\mathrm{mod}\,el} = 46\,mm \cong h_{obstacles} = 50\,mm$).

5.3.3 Standard deviation profile

Finally, a last aspect was checked already with the chosen arrangement. This aspect was the ratio of the standard deviations. According to the used guideline, for the standard deviation it has to be true, that:

$$\sigma_u : \sigma_v : \sigma_w = 1 : 0.75 : 0.5\,, \tag{5.2}$$

where σ_u, σ_v, and σ_w are the standard deviation of the respective velocity component [m/s]

The height dependence of the standard deviation of velocity component *u* and *w* can be seen in figure 5.8.

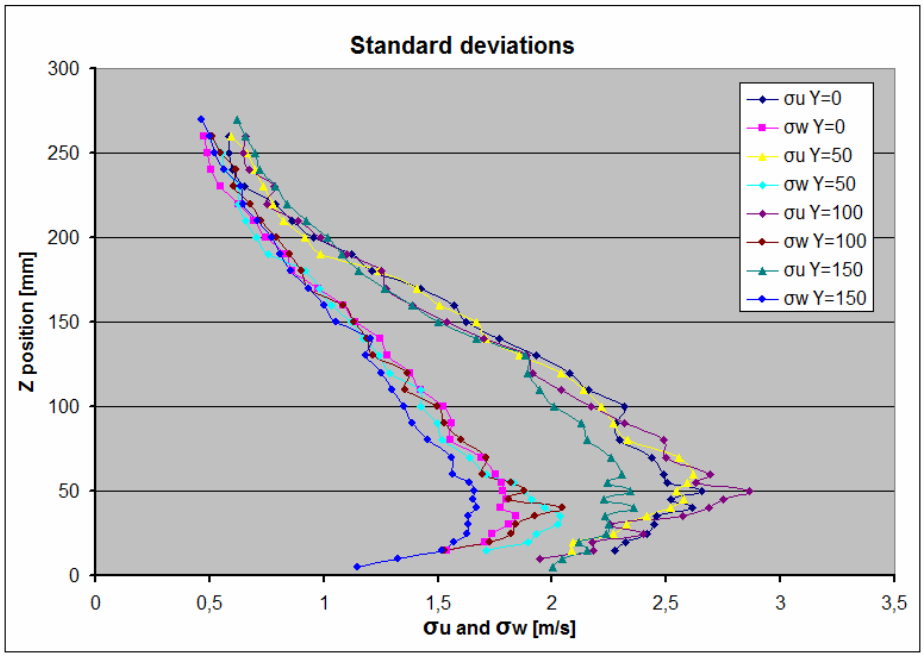

Figure 5.8: *The measured RMS values along a vertical profile*

If we take the average value of each point along the profiles σ_u and σ_w and divide them, then we get a ratio of $\sigma_u : \sigma_w = 1 : 0.712$ which should be around $1 : 0.5$. This ratio still could be improved in the future, but now it is considered acceptable.

5.4 Results of measurement settings

Finally a detailed measurement was done with the final arrangement introduced in the previous chapter (less dense arrangement with double obstacle height). This time, 5 horizontal and 5 vertical profiles were measured from the symmetry plane of the wind tunnel to the side wall, assuming symmetric flow conditions. The measurement location in *x* direction was at 100 *mm* downstream of the boundary layer generator elements. These measurements were then post processed by TecPlot. The results can be seen in figure 5.9, where the velocity vectors are plotted colored by their velocity magnitude.

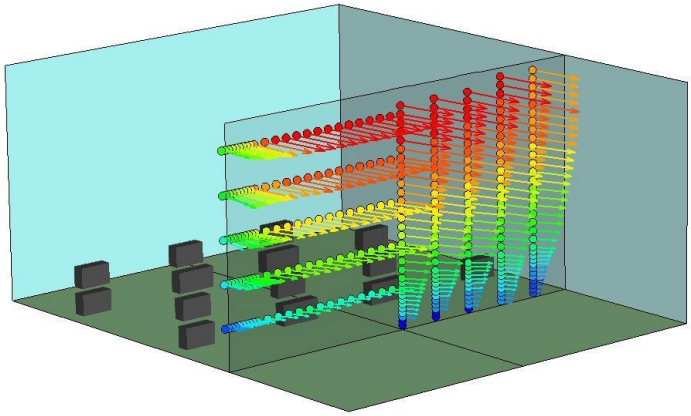

Figure 5.9: *The vector plot of the measured profiles*

In figure 5.9 the horizontal profiles and the vertical profiles can be seen next to each other (both of them could be mirrored for the whole section, this representation is only for have a clear view). We can see how the velocities are breaking down close to wall regions.

To have an expression about overall flow field patterns, interpolated results were calculated from the pointwise measurements to show the field distribution of different variables in the measurement cross section. The interpolation method was an inverse-distance method calculated from the 12 nearest point, with an exponent of 3.5. Figure 5.10 shows the interpolated result of the vertical velocity component (*w*).

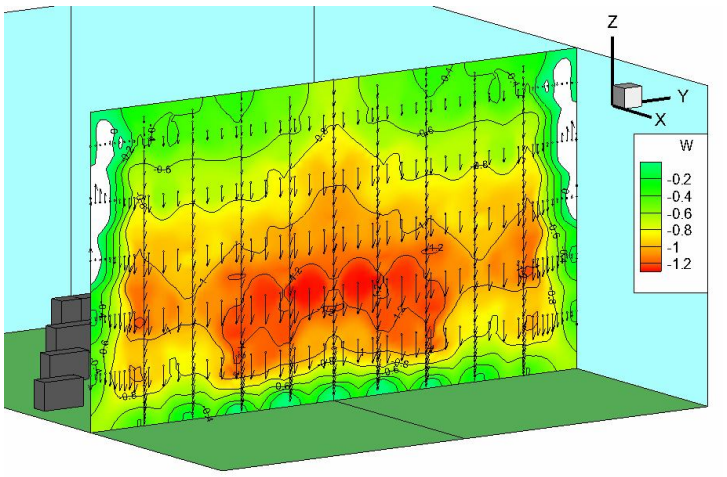

Figure 5.10: *The vertical vector plot and interpolated w field*

Figure 5.10 demonstrates only the vertical components of the velocity vectors, which show a strong downwash almost all around the measurement cross section. The only upward pointing velocities can be noticed in the side wall region (colour cut off region, white). This downwash velocity can be caused also by a secondary vortex or a leak flow from the upper part of the wind tunnel. This effect is planned to be eliminated during future measurements.

The interpolated results of velocity in mean flow direction (u) and turbulence in mean flow direction (I_u) are presented in figure 5.10.

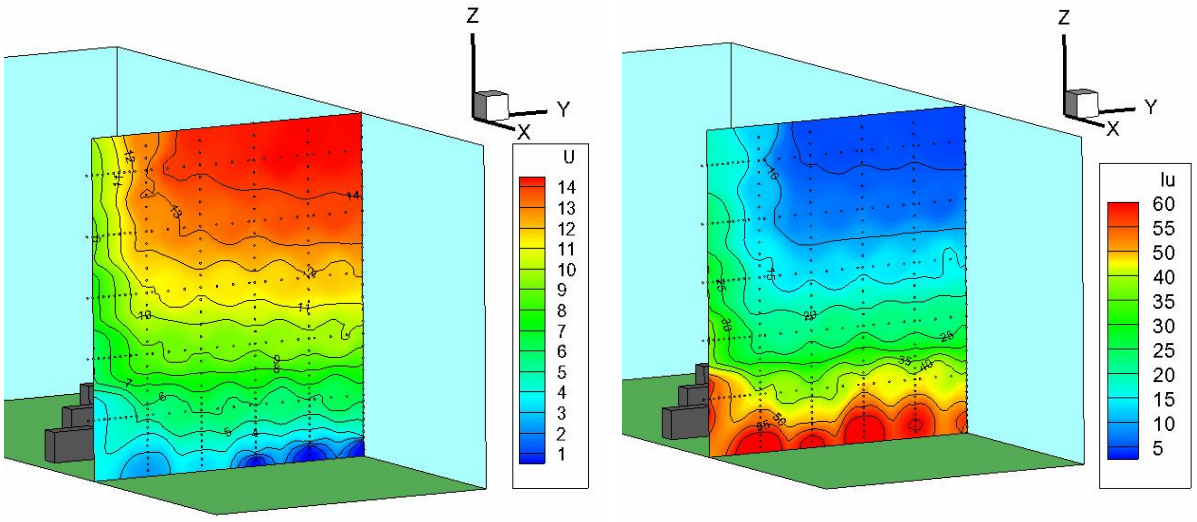

Figure 5.11: *The interpolated velocity (left) and turbulence field (right)*

It can be seen, that the flow reaches its maximum velocity at maximum height in the middle region, and also can be observed, how it slows down close to the walls. The flow can be considered closely uniform at a certain height, the waving interpolation lines can be put down to the interpolation error.

The other picture (on the right side) shows the interpolated turbulence field. As it was expected, the highest turbulence is at the bottom region, in the wake of the boundary layer generator elements, where it reaches at about 60%. A lower, but increased turbulence of 25 - 30 % can also be observed close to the side wall of the wind tunnel.

These results given in chapter 5 provided us reliable measurement conditions similar to real urban flow conditions for the measurement with the real model. This measurement are introduced in chapter 6.

6. MEASUREMENT RESULTS

After determining the proper arrangement of the obstacles to get the best possible inlet flow conditions, the measurement of the modelled urban square could be carried out. We performed measurements from side view through the side window of the wind tunnel and with one wind direction (North wind direction). From side view we can measure the velocity in the main flow direction and in the vertical direction. Thus we could measure profiles in vertical direction to show the variation of the velocity vectors and to define turbulence properties along these profiles.

The goal of the measurement was to have an impression about the flow field of the model and to show some results. The essence of the measurements remains to be done in the next semester. Due to the lack of time, we could carry out only one measurement with the realized wooden model.

During this measurement, three vertical profiles were measured: one in the middle of the *y* plane, 100 mm before the first block, one at the leading edge of the first block, and one at the trailing edge of the same block. Measurement points were situated with an upward decreasing density, 2 *mm* from each other in the lower region, 5 *mm* from each other in the middle region, and finally 10 *mm* from each other.

The model and the location of the measured velocity profiles with velocity vectors are illustrated in figure 6.1.

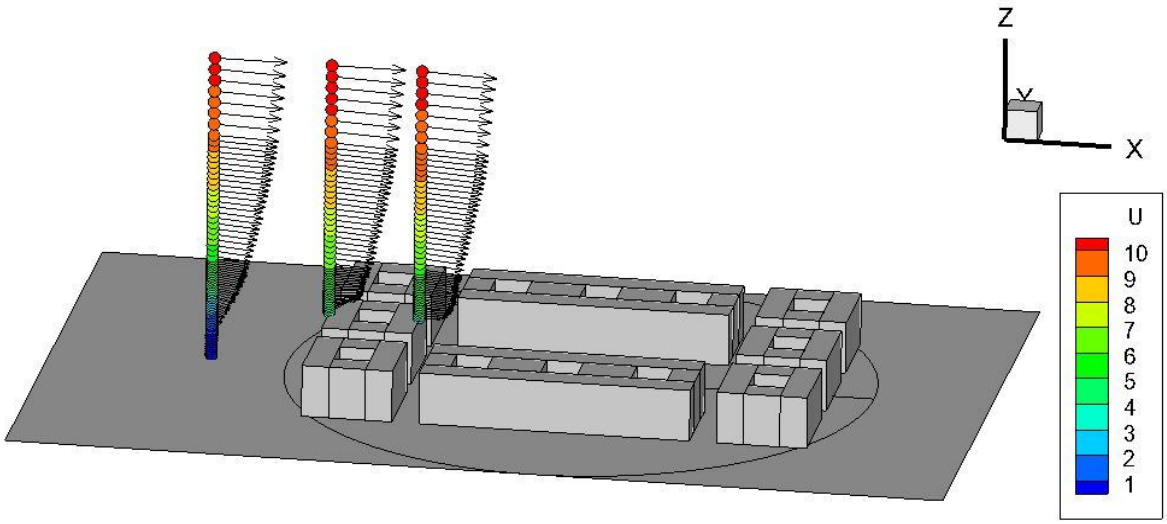

Figure 6.1: *The location of the examined vertical profiles*

The measurement points are coloured according to their velocity in main flow direction. The enlarged profiles with the velocity vectors are shown in figure 6.2. Points are coloured by u velocity and I_u turbulence intensity.

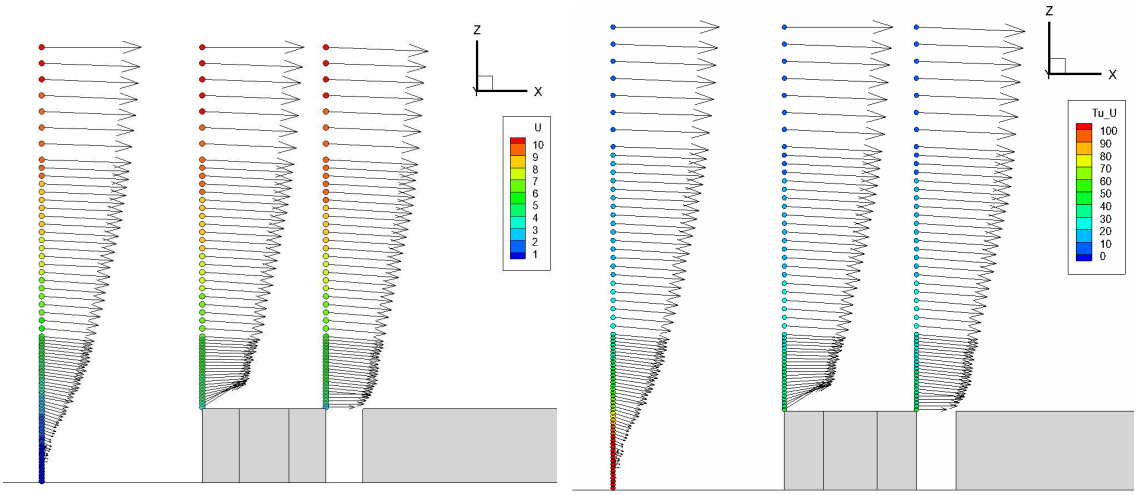

Figure 6.2: *The side view of the velocity vectors with measurement points coloured by main velocity component (left) and main turbulence component (right) along the vertical profiles*

In the first profile, upstream the block, a strong downwash can be noticed especially in the lower region. This is caused by a rectangular boundary layer generator element behind the profile. This region is in the separation zone of that element.

At the leading edge of the bloc, in the bottom of the second profile, the beginning of a separation zone can be observed according to the huge vertical velocity component pointing upward. The velocity magnitude is larger than it would be in the undisturbed case, so acceleration happens at that region.

In the third profile, at the trailing edge the first 5 point in the lower region could not be completely measured. As the vertical laser beam pair was uncovered by the block, the vertical components could not be measured here. Despite, we can observe, that the separation bubble has already reattached, as there is no backflow (the time averaged mean flow velocity component is large enough to declare it).

Furthermore, a recognizable downwash can be noticed all along the profiles. This phenomenon was already observed in chapter 5.4, and possibly it is caused by a secondary vortex or a leak flow from the upper part of the wind tunnel.

We can see in figure 6.2 (right), how the turbulence intensity grows close to the model and the wall. In the first profile (upstream the block) a very strong turbulence can be noticed, almost 100% up to the model height. This is presented because the lower side of the profile is in a separation zone of a boundary layer generator element. In the second and third profiles over the block a turbulence intensity of 30-40% can be seen.

7. SUMMARY

In this semester we defined the examined case, and had a broad literature overview about the topic of wind and dispersion in urban areas. Relating articles were collected and a comprehensive table was made of them.

For the wind tunnel measurements, according to literature guidelines and data, we checked different arrangements of rectangular boundary layer generator elements to get the best possible inlet flow conditions that are really close to that of in real urban areas. For velocity measurement, a Laser Doppler Anemometer was used, whose working principle and features were introduced.

The arrangement and exact dimensions of our investigated model were designed, and the model was prepared from wood. After getting the proper inlet flow conditions in wind tunnel we carried out some profile measurements on the model at North wind direction. The results of this measurement were reported, and further future objectives to do in the next semester were formulated (see chapter 8.).

8. FUTURE PLANS

Next semester we are going to carry out several measurements also from side view to get vertical plane velocity fields and also from upper view to get horizontal plane velocity fields inside the square. We are going to investigate different wind directions and discovering the changing flow patterns. Also we may investigate the effect of wind speed. The supposed change of wind field due to the ventilation system entrance of an underground car park situated underneath the square is also planned to be measured by LDA.

Beyond measuring the whole velocity and turbulence field around the square, we are going to investigate it with another method too, by numerical calculations. The numerical calculation and the measurements can be compared very well, and they are supposed to validate each other.

9. REFERENCES

[1] W. Theurer, 1999. Typical building arrangements for urban air pollution modelling, Atmospheric Environment 33 (1999) 4057-4066

[2] Jane Meri Santos, Neyval Costa Reis, Jr., Elisa Valentim Goulart, Ilias Mavroidis, 2009. Numerical simulation of flow and dispersion around an isolated cubical building: The effect of the atmospheric stratification, Atmospheric Environment 43 (2009) 5484–5492

[3] Parra M.A., Santiago J.L., Martín F.b, Martilli A., Santamaría J.M., 2010. A methodology to urban air quality assessment during large time periods of winter using computational fluid dynamic models, Atmospheric Environment, 44 (2010) 2089-2097

[4] R. W. Macdonald, R. F. Griffiths, D. J. Hall, 1998, An improved method for the estimation of surface roughness of obstacle arrays, Atmospheric Environment, PII: S1352-2310(97)00403-2

[5] Y. Cheng, F.S. Lien, E. Yeeb, R. Sinclair, 2003. A comparison of large Eddy simulations with a standard k–e Reynolds-averaged Navier–Stokes model for the prediction of a fully developed turbulent flowover a matrix of cubes, Journal of Wind Engineering and Industrial Aerodynamics 91 (2003) 1301–1328

[6] R. W. Macdonald, R. F. Griffiths, D. J. Hall, 1998. A comparison of results from scaled field and wind tunnel modelling of dispersion in arrays of obstacles, Atmospheric Environment, PII: S1352-2310(98)0089-2

[7] S.R. Hanna, S. Tehranian, B. Carissimo, R.W. Macdonald, R. Lohner, 2002. Comparisons of model simulations with observations of mean flow and turbulence within simple obstacle arrays, Atmospheric Environment 36 (2002) 5067–5079

[8] P. Neofytou, M. Haakana, A. Venetsanos, A. Kousa, J. Bartzis, J. Kukkonen, 2007. Computational Fluid Dynamics modelling of the pollution dispersion and comparison with measurements in a street canyon in Helsinki, Environ Model Assess (2008) 13:439–448 DOI 10.1007/s10666-007-9110-x

[9] T. Stathopulos, B.A. Baskaran, 1996. Computer simulation of wind environmental conditions around buildings, Engineering structures, 0141-0296(95)00155-7 Cheng-Hsin Chang, Robert N. Meroney, 2003.

[10] The effect of surroundings with different separation distances on surface pressures on low-rise buildings, Journal of Wind Engineering and Industrial Aerodynamics 91 (2003) 1039–1050

[11] Jae-Jin Kim, Jong-Jin Baik, 2002. Effects of inflow turbulence intensity on flow and pollutant dispersion in an urban street canyon, Journal of Wind Engineering and Industrial Aerodynamics 91 (2003) 309–329

[12] Mavroidis, R.F. Griffiths, D.J. Hall, 2003. Field and wind tunnel investigations of plume dispersion around single surface obstacles, Atmospheric Environment 37 (2003) 2903–2918

[13] R.W. Macdonald, R.F. Griffiths, S.C.Cheah, 1996. Field experiments of dispersion through rectangular arrays of cubic structures, Atmospheric environment PII:S1352-2310(96)00263-4

[14] Young-Hee Ryu, Jong-Jin Baik, 2009. Flow and dispersion in an urban cubical cavity, Atmospheric Environment 43 (2009) 1721–1729

[15] L. Soulhac, V. Garbero, P. Salizzoni, P. Mejean, R.J. Perkins, 2009. Flow and dispersion in street intersections, Atmospheric Environment 43 (2009) 2981–2996

[16] H. Cheng, P. Hayden, A.G. Robins, I.P. Castro, 2007. Flow over cube arrays of different packing densities, Journal of Wind Engineering and Industrial Aerodynamics 95(2007) 715–740

[17] Marko Princevac, Jong-JinBaik, XiangyiLi, HanshengPan, Seung-BuPark, 2010. Lateral channeling within rectangular arrays of cubical obstacles, Journal of Wind Engineering and Industrial Aerodynamics 98 (2010) 377–385

[18] Zheng-Tong Xie, Ian P. Castro, 2009. Large-eddy simulation for flow and dispersion in urban streets, Atmospheric Environment 43 (2009) 2174–2185

[19] Mavroidis, R.F. Gri$ths, 2000. Local characteristics of atmospheric dispersion within building arrays, Atmospheric Environment 35 (2001) 2941}2954

[20] O. Coceal, T.G. Thomas, I.P. Castro, S.E. Belcher, 2006. Mean flow and turbulence statistics over groups of urban-like cubical obstacles, Boundary-Layer Meteorol (2006) 121:491–519 DOI 10.1007/s10546-006-9076-2

[21] Yi Yang, Ming Gu, Suqin Chen, Xinyang Jin, 2009. New inflow boundary conditions for modelling the neutral equilibrium atmospheric boundary layer in computational wind engineering, Journal of Wind Engineering and Industrial Aerodynamics 97 (2009) 88–95

[22] A. Gadilhe, L. Janvier, G. Barnaud, 1993. Numerical and experimental modelling of the three-dimensional turbulent wind flow through an urban square, Journal of Wind Engineering and Industrial Aerodynamics, 46 & 47 (1993) 755-763

[23] Jae-Jin Kim, Jong-Jin Baik, 2004. A numerical study of the effects of ambient wind direction on flow and dispersion in urban street canyons using the RNG k–e turbulence model, Atmospheric Environment 38 (2004) 3039–3048

[24] D.M. Hargreaves, N.G. Wright, 2007. On the use of the k–ε model in commercial CFD software to model the neutral atmospheric boundary layer, Journal of Wind Engineering and Industrial Aerodynamics 95 (2007) 355–369

[25] R.N. Meroney, 1999. Perspectives on air pollution aerodynamics, Plenary Session Paper, 10th International Wind Engineering Conference, Copenhagen, Denmark, June 21-25, 1999

[26] W. Theurer, E. J. Plate, K. Hoeschele, 1996. Semi-empirical models as a combination of wind tunnel and numerical dispersion modelling, *Atmospheric Environment,* PII: S1352-2310(96)00072-6

[27] David Hamlyn, Trevor Hilderman, Rex Britter, 2007. A simple network approach to modelling dispersion among large groups of obstacles, Atmospheric Environment 41 (2007) 5848–5862

[28] Robert N. Meroney, Michel Pavageau, Stilianos Rafailidis, Michael Schatzmann, 1996. Study of line source characteristics for 2-D physical modelling of pollutant dispersion in street canyons, Journal of Wind Engineering and Industrial Aerodynamics 62 (1996) 37-56

[29] David K. Heist, Jennifer Richmond-Bryant, Laurie A. Brixey, George E. Bowker, Steven G.Perry, Russell W. Wiener, 2009. The effect of a tall tower on flow and dispersion through a model urban neighborhood, Part 1. Flow characteristics, Journal of Environmental Monitoring 2009, 11, 2163-2170, DOI: 10.1039/B907135K

[30] Laurie A. Brixey, Jennifer Richmond-Bryant, David K. Heist, George E. Bowker, Steven G.Perry, Russell W. Wienere, 2009. The effect of a tall tower on flow and dispersion through a model urban neighborhood, Part 2. Pollutant dispersion, Journal of Environmental Monitoring 2009, 11, 2171-2179, DOI: 10.1039/B907137G

[31] Cheng-Hsin Changa, Robert N. Meroney, 2003. The effect of surroundings with different separation distances on surface pressures on low-rise buildings, Journal of Wind Engineering and Industrial Aerodynamics 91 (2003) 1039–1050

[32] Jae-Jin Kim, Jong-Jin Baik, Hye-Yeong Chun, 2001. Two-dimensional numerical modeling of flow and dispersion in the presence of hill and buildings, Journal of Wind Engineering and Industrial Aerodynamics 89 (2001) 947–966

[33] Luca Delle Monache, Jeffrey Weil, Matthew Simpson, Marty Leach, 2009. A new urban boundary layer and dispersion parameterization for an emergency response modeling system: Tests with the Joint Urban 2003 data set, Atmospheric Environment 43 (2009) 5807–5821

[34] Robert N. Meroney, Bernd M. Leitl, Stillianos Rafailidis, Michael Schatzmann, 1999. Wind-tunnel and numerical modeling of flow and dispersion about several building shapes, Journal of Wind Engineering and Industrial Aerodynamics 81 (1999) 333-345

[35] Michel Pavageau, Michael Schatzmann, 1999. Wind tunnel measurements of concentration fluctuations in an urban street canyon, Atmospheric Environment 33 (1999) 3961-3971

[36] K. Ahmada, M. Khareb, K.K. Chaudhryc, 2005. Wind tunnel simulation studies on dispersion at urban street canyons and intersections—a review, Journal of Wind Engineering and Industrial Aerodynamics 93 (2005) 697–717

[37] M. J. Davidson, W. H. Snyder, R. E. Lawson, J. C. R. Hunt, 1996. Wind tunnel simulations of plume dispersion through groups of obstacles, Atmospheric Environment, PII: S1352-2310(96)00103-3

[38] VDI-Richtlinien, 2000. VDI 3783 Blatt 12, Verein Deutscher Ingenieure

[39] Tropea, Cameron; Yarin, Alexander L.; Foss, John F., 2007. Springer Handbook of Experimental Fluid Mechanics, XXVIII, 1557 p. 1240 illus. in color, ISBN 978-3-540-30299-5

[40] Phase Doppler Particle Analyzer (PDPA)/Laser Doppler Velocimeter (LDV), TSI Operation Manual, P/N 1990048, Revision D, November 2005

[41] FSA Multi-bit Digital Processors, TSI Operation Manual, P/N 1990016, Revision A, 2004.

[42] A Family of Laser and Phase Doppler Measurement Systems Providing Unmatched Flexibility and Patented Technology, TSI Operation Manual, P/N 5001100, Revision A, 2007.

[43] PDM Scattered Light Separation and Photodetector System, TSI Operation Manual, P/N 1990036, Revision B 8/05, 2005.

[44] Multicolor Beam Separator, TSI Operation Manual, P/N 1990035, Revision A, 2002.

10. APPENDIX

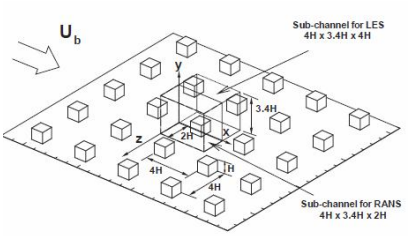

figure 1

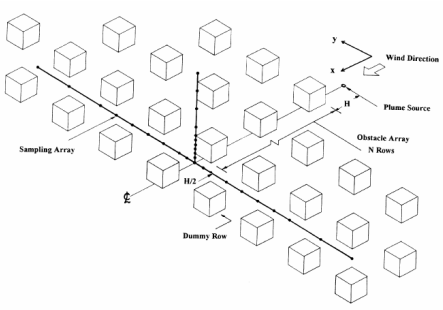

figure 2

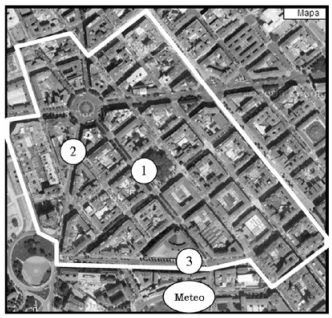

figure 3

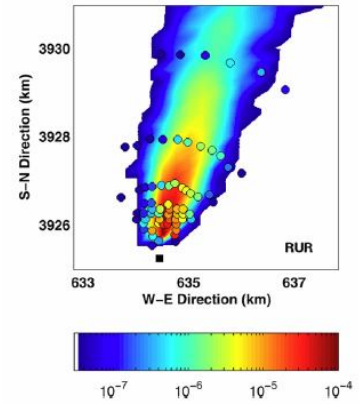

figure 4

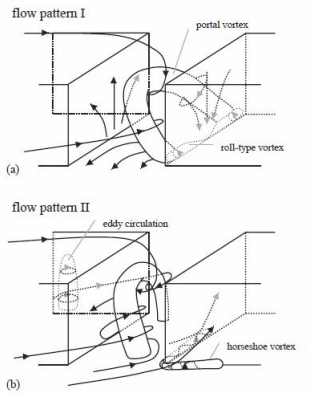

figure 5

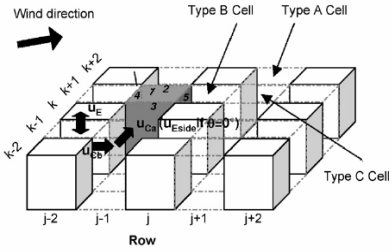

figure 6

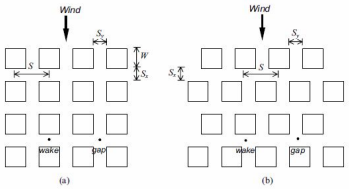

figure 7

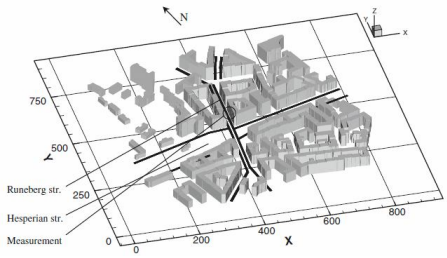

figure 8

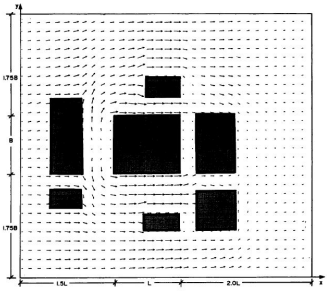

figure 9

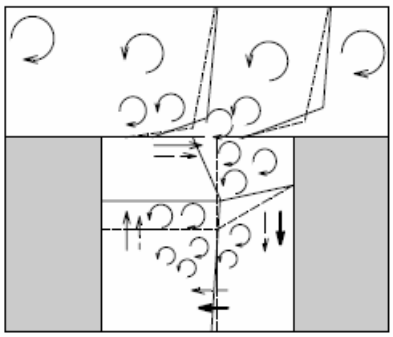

figure 10

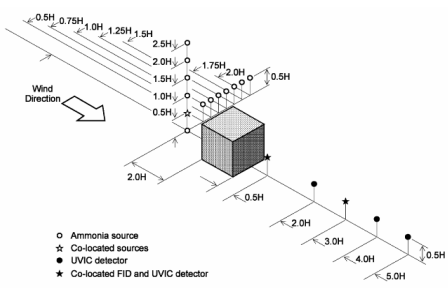

figure 11

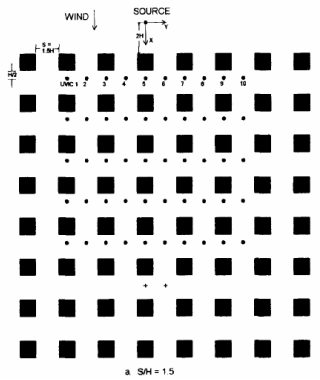

figure 12

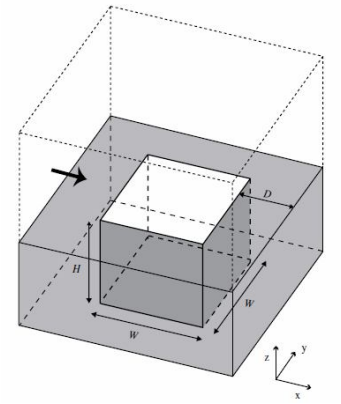

figure 13

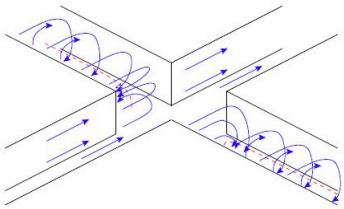

figure 14

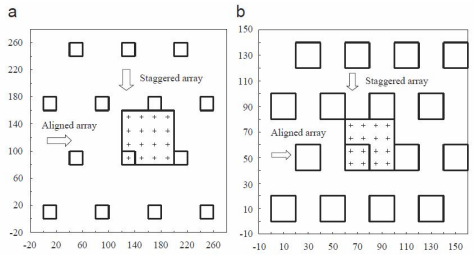

figure 15

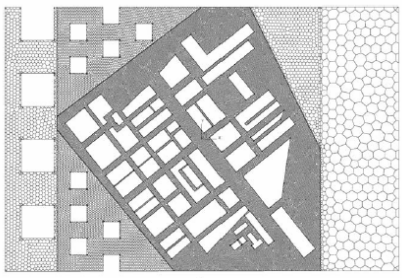

figure 16

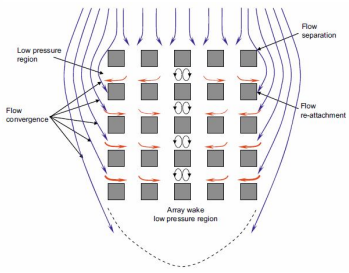

figure 17

figure 18

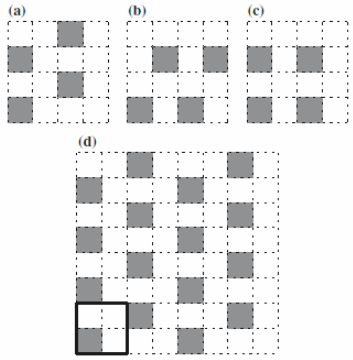

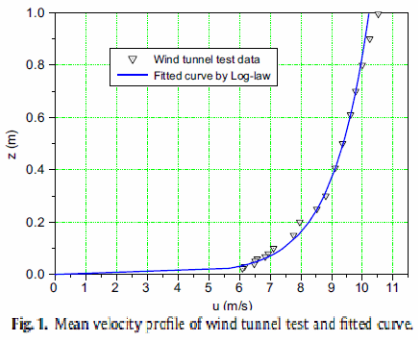

Fig. 1. Mean velocity profile of wind tunnel test and fitted curve.

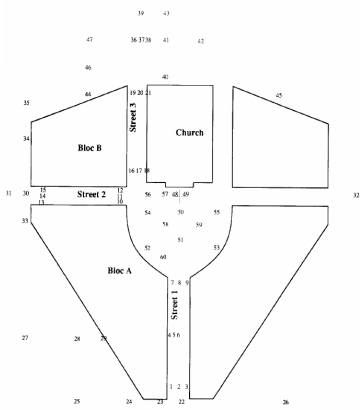

figure 19 *figure 20* *figure 21*

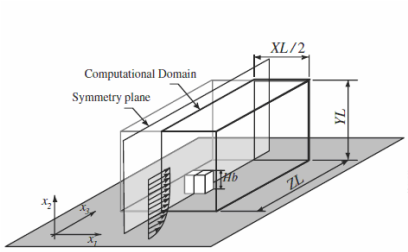

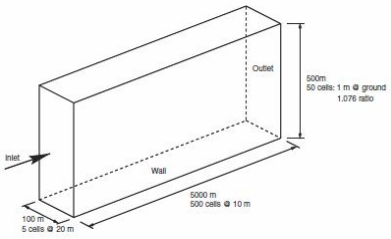

Build. heights H; uniform. λ_H:	20m, 40m; 0.28
Arrangement:	B3
Approach flow:	0°
Alignment ratio λ_{LB}:	4
Buildings packing ratio λ_A:	0.30
Frontal aspect ratio (β = 0°) λ_{FA}:	0.10

figure 22 *figure 23* *figure 24*

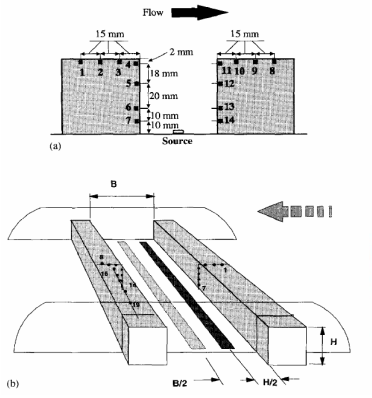

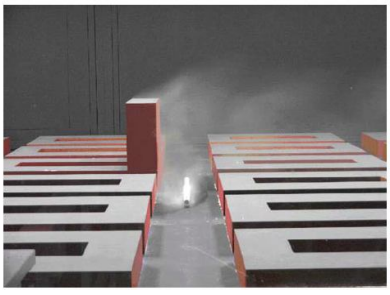

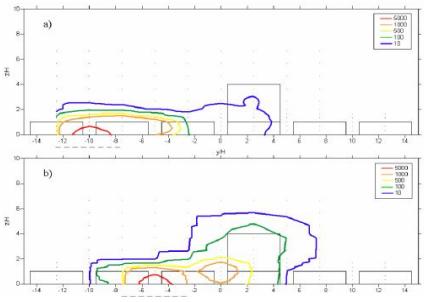

figure 25 *figure 26* *figure 27*

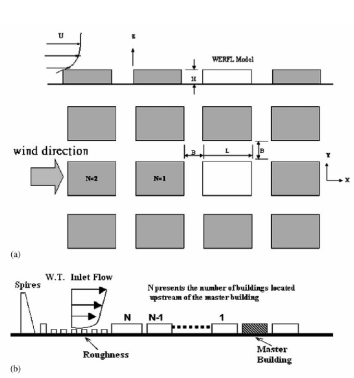

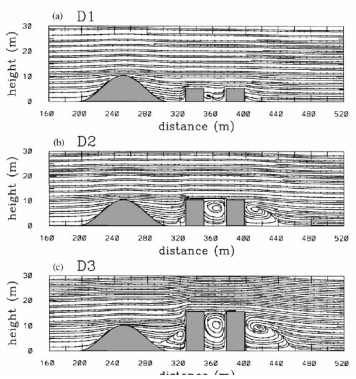

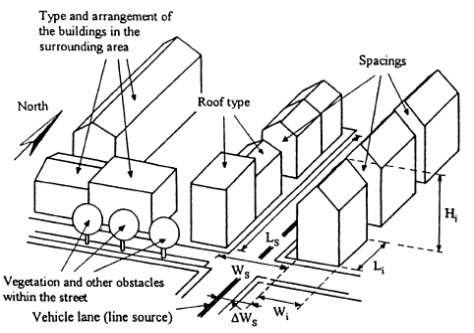

figure 28 *figure 29* *figure 30*

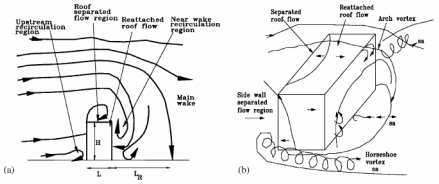

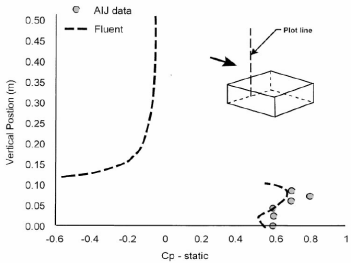

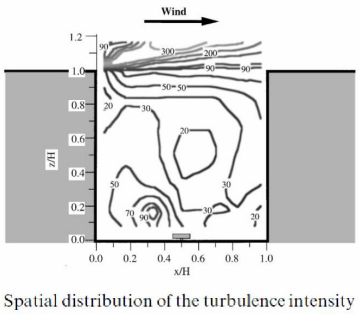

Spatial distribution of the turbulence intensity

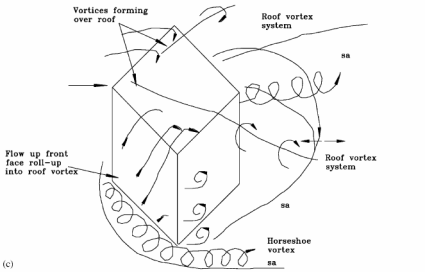

figure 31 *figure 32* *figure 34*

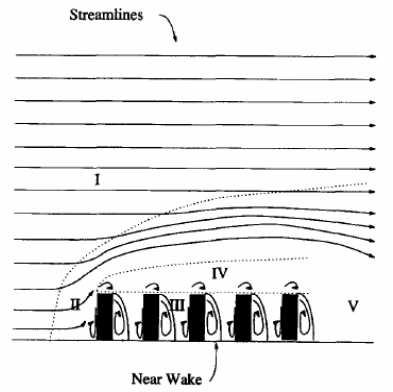

figure 34